OBSERVATIONAL TECHNIQUES FOR SOLAR FLARE GAMMA-RAYS, HARD X-RAYS, AND NEUTRONS

Grant NAGW-516

Robert P. Lin, Principal Investigator

Space Sciences Laboratory
University of California
Berkeley, CA 94720

Final Report for period November 1, 1983–November 30, 1988

April 18, 1989

Summary

This grant covers the development of new instrumentation and techniques for solar hard X-ray, gamma-ray and neutron observations from spacecraft and/or balloon-borne platforms. The principal accomplishments are: (1) the development of a two-segment germanium detector which is near-ideal for solar hard X-ray and gamma-ray spectroscopy; (2) the development of long duration balloon flight techniques and associated instrumentation; and (3) the development of innovative new position-sensitive detectors for hard X-ray and gamma-ray.

I. Introduction

This grant covers the development of innovative new instrumentation and techniques for hard X-ray, gamma-ray, and neutron observations from spacecraft and/or balloon-borne platforms in the next solar maximum. The motivation for this development comes from the numerous new and exciting results from high energy observations during the previous solar maximum, including:

1) The discovery that numerous flares produce gamma-ray line and continuum emission characteristic of accelerated nuclei (see *Chupp*, 1986), suggesting that ion acceleration may occur in essentially all solar flares.

2) The discovery of the near simultaneity of the gamma-ray emission to the impulsive $10–10^2$ keV hard X-ray burst, indicating that the acceleration of ions to $\gtrsim 10–10^2$ MeV also occurs rapidly (within seconds) in flares.

3) The first observations of energetic (50–500 MeV) neutrons and >10–100 MeV gamma-rays from solar flares (*Chupp et al.*, 1982).

4) The discovery that flares which emit >10 MeV gamma-rays are all located near the solar limbs, indicating an apparent strong directivity in the gamma-ray emission.

5) The discovery of a new component of hard X-ray emission with a very steep, close to isothermal spectrum which dominates the energy range below ~30–35 keV (*Lin et al.*, 1981).

6) The observations of brightening in hard, 20–30 keV X-rays of the *footpoints* of flare loops, providing the first direct evidence for non-thermal electron beams (*Hoyng et al.*, 1981).

7) In contrast, the VLA radio imaging of flare microwave emission, which is presumably produced by ≳100 keV electrons, shows brightening at the *tops* of the flare loops (*Marsh and Hurford*, 1980).

8) The first high resolution spectral measurements of "normal" impulsive solar flare hard X-ray bursts, which show that the spectral shape is dominated by double power-law spectra with relatively sharp breaks (*Lin and Schwartz*, 1986). These spectra suggest that acceleration of the non-relativistic electrons, which may contain a significant fraction of the energy released in a flare, may be due to dc electric fields.

9) The discovery of hard X-ray microflares, bursts with X-ray fluxes $10–10^2$ times smaller than normal flares which occur about once every five minutes near solar maximum (*Lin et al.*, 1984). These microflares indicate that even very small transient releases of energy by the Sun may be non-thermal in origin.

In the best tradition of good astrophysics, these discoveries have raised a host of new scientific questions which can be answered only with new and improved measurements.

Under this grant we have concentrated our efforts in three areas: (1) the development of a near-ideal detector for solar hard X-ray and gamma-ray spectroscopy, (2) the development and fabrication of instrumentation for long duration balloon flights, and (3) the development of position-sensitive detectors for hard X-ray and gamma-ray imaging and polarization measurements.

II. Gamma-ray, Hard X-ray, and Neutron Spectroscopy

Gamma-ray Line Spectroscopy

Gamma-ray emission from the Sun results from the interactions of energetic protons, nuclei and electrons with the solar atmosphere (see *Ramaty et al.*, 1975; *Ramaty*, 1986 for review). These interactions produce gamma-ray lines from the captures, annihilations and de-excitations of neutrons, positrons and excited nuclear levels, respectively, and continuum emission from bremsstrahlung of relativistic electrons, pi meson decays, and Doppler-broadened nuclear lines. The observation of these gamma-rays provides unique information on high energy processes at the Sun, including properties of energetic particles such as the timing of their acceleration, the ratio of electrons to protons, and the number, energy spectrum, chemical composition and possible beaming of the particles.

Solar gamma-ray spectroscopy also offers the possibility of determining abundances in the solar atmosphere. *Murphy et al.* (1985) have already shown from the SMM gamma-ray spectrometer (GRS) data that the abundances in the gamma-ray production region differ significantly from photospheric abundances. High resolution gamma-ray spectroscopy could determine the relative abundances of C, O, Mg, Si, and Fe in the corona, with accuracy that could match or even exceed that of atomic spectroscopy. Gamma-ray line observations could also determine the photospheric ^{3}He abundance, a quantity which cannot be obtained in any other way. Moreover, the origin of ^{3}He in ^{3}He-rich flares is still not well understood, and gamma-ray observations could provide clues to the origins of these spectacular isotopic enrichments in energetic solar particles.

One of the major advances in our knowledge of solar flares has come from the recent gamma-ray observations of the Solar Maximum Mission (SMM), and, to a lesser extent, of the Japanese satellite, HINOTORI. These show that solar flares often accelerate ions to energies of $\gtrsim$10 MeV up to GeV, which in turn produce a wide variety of gamma-ray lines through collisions with the ambient medium (*Chupp*, 1983). The timing of the gamma-ray emission relative to the hard X-ray emission indicates that the acceleration of ions often occurs in close coincidence with the impulsive acceleration of the electrons. These observations suggest the possibility that the acceleration of ions occurs in essentially all flares and that the same process accelerates both

electrons and ions in the flare impulsive phase.

High spectral resolution measurements are required to exploit the information residing in the gamma-ray line and continuum spectrum. Figure 1 shows that the resolution of NaI is broader than the expected widths for essentially all the lines, while the resolution of liquid nitrogen-cooled germanium semiconductor detectors is sufficient to measure accurately all the parameters of the gamma-ray lines (with the possible exception of the neutron capture deuterium line at 2.223 MeV, whose width is ~0.1 keV). In the next solar maximum, it would be desirable to be able to do good high resolution spectroscopy not just for the very large flares, but also for smaller flares – i.e., to have sufficient counts to define the spectral line shapes (centroids, widths, and more detailed information). Thus large, effective detector areas are required.

A strawman instrument consisting of an array of nineteen 6.5 cm dia×6.5 cm long germanium coaxial detectors would have an effective area of about twice that of SMM, and a total Ge volume of about 4100 cm^3. If this array is actively shielded and collimated as well as the best current cosmic gamma-ray instruments, the background in the 200 keV to 2 MeV range would contribute ~$10–10^2$ counts/keV during a solar gamma-ray burst of typical duration of ~10^3 seconds. Using the new, innovative Ge detectors and pulse shape analysis techniques developed under the present grant, we expect to be able to reduce this background by a factor of at least 10, and to improve the 3σ line sensitivity for flares by a factor of ~2 to 4, depending on the line width and shield leakage background levels.

A gain in sensitivity is also obtained for narrow lines by the high energy resolution of a Ge system. In the case where the number of background counts is $\gg 1$, i.e., where Gaussian statistics apply, and the observation is background-limited, the minimum detectable line flux is given by:

$$F_L = (1.30\, k/\epsilon M)\,[BW/(1/T_s + 1/T_B)\,A]^{1/2}\ \mathrm{ph/cm^2-sec}$$

Here k is the statistical criterion (number of standard deviations); ϵ, the detector efficiency for total absorption of gamma-rays (or 1st or 2nd escape peak, in the case of pair production); M, the on-/off-source modulation efficiency; B, the detector background per unit energy and geometric area exposed to the source; S, the line width or detector energy resolution (FWHM), whichever is greater; A, the geometric detector area; and T_s and T_B, the times collecting source (plus background) and background data. Since the line widths are generally less than the resolution width of NaI but greater than that of Ge, there is a significant gain in line sensitivity for Ge. For example, for the 2.223 MeV deuterium line with intrinsic width of about 0.1 keV, germanium (2.1 keV resolution) is more sensitive than NaI (~90 keV resolution) by a factor of $(90/2.1)^{1/2}$ =6.5 for the same effective area.

With improved sensitivity and energy resolution quantitative gamma-ray spectroscopy (as opposed to just line detection) can be done for the first time in astrophysics.

Hard X-ray and Gamma-ray Continuum

Almost all of the measurements of solar flare hard X-ray and gamma-ray burst continuum spectra have been made with scintillation detectors. The poor energy resolution of these detectors inherently limits the steepness of the continuum spectra that can be measured. Furthermore, the observed spectra must be deconvolved by assuming an *a priori* spectral shape, convolving it with the detector response, and comparing the result with the actual observed count rate spectrum. As pointed out by *Fenimore et al.* (1982), this procedure can lead to artifacts in the spectra. In addition, small changes in gain and/or dead layers will strongly affect the results. Finally, nonlinearities and K-edge effects in the middle of the hard X-ray range further complicate the interpretation of the spectra.

The advantages of high resolution germanium detectors for solar hard X-ray spectroscopy are evident from our 27 June 1980 balloon flight, when a medium-size solar hard X-ray burst was observed. We discovered immediately that a nearly isothermal component dominated the spectrum below ~30 keV (*Lin et al.*, 1981). Such a component has a spectral power-law slope as steep as ~−11, far too steep to be measured by scintillators (see Figure 1). HINOTORI and SMM have confirmed the existence of this component through continuum observations at lower energies and through Fe^{XXVI} line measurements. This component appears to be a common feature in flares.

The spectral measurements of the "normal" impulsive phase hard X-ray burst in the same flare showed that the dominant spectral shape is a double power-law with a relatively sharp break (*Lin and Schwartz*, 1987). Emission from an isothermal 10^8–10^{9}°K plasma can be specifically excluded. The double power-law shape suggests that dc electric field acceleration, with total potential drops of ~10^5 volts, may be the source of the energetic electrons which produce the hard X-ray emission in flares. The hard X-ray emission could be observed at a very low level for at least 20 minutes after the impulsive phase, indicating that trapping of the electrons high in the corona and/or long-lived continuous acceleration may be occurring. At that point the flux was only a fraction of the diffuse sky background in the 3°×6° detector aperture.

On the same balloon flight ~25 hard X-ray bursts with peak fluxes a factor of 10–10^2 smaller than normal flare events were observed in 141 minutes of solar observation (*Lin et al.*, 1984). These hard X-ray microflares last a few seconds to tens of seconds and have power-law energy spectra. These observations suggest that even very small transient energy releases by the Sun may be non-thermal in character. High sensitivity, comparable to cosmic hard X-ray instruments, is clearly desirable for solar observations.

Germanium Detector Development

Under this grant we have developed a germanium detector with the following features:

1) It is capable of measuring the entire energy range from ~10 keV to ≳10 MeV.

2) It has very high energy resolution (~0.5 keV at 50 keV to ~5 keV at 10 MeV).

3) It can reject with very high efficiency the β-decay radioactivity in the detector itself, which is the dominant source of background in the 200 keV–3 MeV range for well-shielded detectors.

4) Its background at lower energies, 10 keV–200 keV, is comparable to that of the best phoswich scintillation detector system.

5) It is highly linear and intrinsically stable in gain.

6) It is highly reliable and relatively insensitive to contaminants and to handling. These characteristics make large arrays of detectors feasible.

The low background is achieved at low energies, ~10 to ~200 keV, by electrically segmenting the detector to provide the germanium equivalent of a phoswich scintillation detector (Figure 2); at high energies, ≳200 keV, it is achieved by reducing the background from detector radioactivity which consists mainly of β-decays. This is done by distinguishing single- from multi-site events throughout the detector volume. Radioactive decays of β-particles are single-site events. At energies below ~150 keV, where photoelectric absorption is dominant, incident photon absorption is also single-site (neglecting the short range of K X-rays). Photons at higher energies, because of Compton scattering, and annihilation photon absorption following pair production, typically have multiple site energy loss signatures.

The resulting germanium detector, shown schematically in Figure 2, has a closed-end coaxial geometry and is made of n-type material, ~6 cm in diameter and ~6 cm thick. As larger diameter detectors become feasible in the next few years, we will use them. Germanium of n-type is used because detectors made with it are essentially immune to radiation damage from fluxes of energetic particles in a several-year space mission (*Pehl*, 1978).

The detector has multiple collecting electrodes which divide it into two distinct volumes, or segments, according to the electrical field pattern. In the central 1.0 cm diameter hole which extends to within ~8 mm of the top, two separate contacts are provided by diffusing lithium into the germanium, coating the lithium with gold, then lapping away the gold in the boundary between the contacts. The detector is then re-etched to provide a clean surface in the boundary; the gold is unaffected by the etch (*Luke*, 1984). The top contact collects charge from the upper 1.5 cm segment of the detector, and the long lower contact collects charge from the bottom ~4.5 cm coaxial segment. The outer and top surfaces are implanted with boron to make a very thin window for X-rays, and metallized for the high voltage contact. The bottom flat surface of the

detector is coated with amorphous germanium to eliminate surface channeling effects.

During the grant period we have fabricated and tested one 4 cm dia × 4 dia prototype and six 5.5 cm dia × 5.5 cm segmented detectors. Our techniques for the fabrication of these detectors are now well developed and fairly routine.

The detector operates in three low background modes, which are summarized in Table I. The "Front Segment Mode" is used at low energies (≤200 keV) where photoelectric absorption dominates. Photons are absorbed in the front ~1 cm segment, while background is rejected by anticoincidence with the adjacent rear segment of the detector. Therefore, this mode has the excellent background rejection properties of a phoswich type scintillation counter (*Matteson et al.*, 1977). The pancake geometry of the front detector has a substantially lower capacitance than a normal planar detector of the same dimensions, resulting in significantly better energy resolution.

Table I.

Mode	Event Selection Criteria
Front Segment	Energy loss only in the front segment.
Front-Rear Coincidence	Energy loss in both segments. (Requires multiple site event.)
Rear Pulse Shape Discrimination (PSD)	Energy loss only in the rear segment. Pulse shape discrimination accepts only multiple-site events.

Multiple-site interactions will be recognized in two ways. First, gamma-rays, which lose part of their energy in the front segment and the rest in the rear segment, would be identified by front-rear coincidence. Second, in the rear segment, pulse shape discrimination will be used to identify multiple-site interactions (for pure rear segment events) located at different radial distances. Pulse shape discrimination is possible because energy deposited in the Ge detector at a given site produces charge carriers, which travel radially in the electric field of the detector to the central and outer contact. Thus the charge collection, and hence the current pulse at the preamplifier input, depends on the radial location of the site of energy deposition. Typically, charge collection takes up to ~200–350 ns in a 5.5 cm dia detector. When the energy deposition of a multiple-site interaction is distributed in radius, the pulse shape becomes a superposition of single-site pulses.

We have computed the detailed shape of the current pulse waveform for single-site energy losses typical of single photopeak absorption events and β-decay radioactivity, and for the distributions of energy depositions resulting from a Monte Carlo photon propagation program (see *Roth et al.*, 1984). The differences in current pulse waveforms for single site versus multiple-site energy losses can be exploited to provide discrimination between β-decay background and true photons in the energy range ~0.3 to 2 MeV. Below we describe the pulse shape discrimination electronics and

detailed laboratory and balloon flight testing of this technique.

Ge Detector Electronics

In this grant period we have also developed techniques and electronics for fast digital storage and subsequent detailed analysis of the Ge current pulse shape, and methods for producing single-site interactions in the detector for testing. The current pulse is sampled every 10 ns by the circuitry shown in Figure 3.

The signal path from each detector segment to its respective Pulse Height Analyzer (PHA) is straightforward with the following exception: in order to achieve a dynamic range greater than that allowed by the 12-bit PHA, the shaping amplifier contains a switchable 5x attenuator controlled by a discriminator on the preamplifier output line. This extends the range of the PHA on each segment up to 12.5 MeV. The status of the gain switch is latched by the PHA, when triggered, as a 13th data bit.

Pulse shape information was initially obtained by additional circuitry, connected only to the signal path from the coaxial detector segment, consists of a fast differentiator and a LeCroy model 2261 Image Channel Analyzer utilized here as a Pulse Shape Analyzer (PSA). The fast differentiator, with a time constant of 10 ns, extracts the detector current waveform from the preamp output waveform and passes it to the PSA. Later it was realized that a separate preamp to take the shape signal off the high voltage connection to the detector would avoid image charge pulses on the front segment. A separate current preamp has been used for the past two years.

The PSA module consists of a Charge Coupled Device (CCD), support, and readout logic circuitry. The CCD is an analog shift register (sometimes referred to as a charge packet bucket brigade) with a length of 640 cells and a clock speed of 100 Mhz. An input signal is sampled, converted into a charge packet, and shifted at the 100 Mhz rate; thus the time length of the device is 6.4 μs with a resolution of 10 ns. Upon receipt of a Stop signal, the 100 Mhz clock signal is replaced with a 100 KHz clock signal, the charge packets are converted to voltage levels as they arrive at the back of the CCD, and these voltage signals are passed to a 12-bit Analog-Digital Converter (ADC). The 12-bit words are stored in a local memory and become available for readout at the completion of the conversion process. This time dilation capability of the CCD allows a combination of accuracy and time resolution not otherwise possible at this time.

To conserve telemetry, only the first 50 samples of shape data are read out. To insure that the event of interest occurs within these fifty samples the PSA Stop pulse must be issued approximately 6.3 microseconds after the event occurs. This is done in the following manner. The shaping amplifiers were designed to have a peaking time of 6.0 μs. The PHA trigger pulse, generated at the pulse peak, is also passed to an adjustable delay circuit which then supplies the Stop signal to the PSA.

A function and address logic block provides a CAMAC environment for the PSA to function properly without modifications. This scheme utilizing the LeCroy unit was used in the 1988 balloon flight.

For an array of many Ge detectors the high data rate and high power consumption required for digitizing and telemetering the pulse shapes to the ground is impractical, particularly for the high count rates expected for solar flare bursts. In a large solar flare the flux of 0.4–2 MeV gamma-rays would be $\gtrsim 10^2$ $(cm^2\ s^1)^{-1}$ so the counting rate for a 6.5 cm dia$\times$6.5 cm length Ge detector would be ~400 counts/s. Since each pulse shape takes ~500 bits to characterize at 10 ns time resolution, about 200 kbps would be generated for each detector, so an array of 10–20 detectors would generate 2–4 megabits/s. Thus a system to analyze the pulse shape digitally in near-real time to obtain the relevant shape parameters is required. A basic change in Figure 3 is the replacement of the very power hungry (~25 watts) LeCroy 2261 CCD image analyzer with a flash ADC followed by storage into memory. Such a replacement unit has been designed, developed, and fabricated for a balloon flight in spring 1989 for non-solar observations.

We have also made detailed studies of background rejection, dynamic range, active shield, and analog and digital electronics. These are described in detail in Appendix A.

The data from each Ge detector for the high count rates of solar flares would be sort by a dedicated microprocessor operating in near-real time. This microprocessor could be programmed with sophisticated algorithms for ginning the spectroscopy data and analyzing the shape. The shape parameters would then be sent to the data stream together with energy information.

Even so, we estimate $\gtrsim$32 bits per detected photon are required for the energy and shape information, so the data handling electronics would need to accommodate $\gtrsim$12 kilobits/s per detector. For a large flare (duration ~10^3 s) observed by an array of 10–20 Ge detectors, the total amount of data for the 0.4–2 MeV range alone would be ~100 megabits. Together with the hard X-ray information from the front segment, we estimate that on the order of $\gtrsim 2\times 10^8$ bits are generated in a large flare. Thus we have developed a system for handling, storage, and onboard compression of data for our long duration balloon payload. That system is configured so that data can be DMA-input at a rate of ~1 megabyte/s.

It is capable of operating the payload independently for long periods (20 days or more). Its tasks include:

1) collection and storage of the data from the detectors;

2) monitoring the data and generating burst triggers;

3) compression and transmission of the data to geosynchronous spacecraft and to the ground station;

4) computing the gondola location and controlling the pointing of the detectors.

The data system consists of an 80C86 microprocessor, 16 Megabits of RAM memory, a VCR-based data storage system, sun sensors, transmitters, etc. A more detailed description is contained in Appendix B (*Lin et al.*, 1987).

Neutron Detection

During the grant period we have developed Ge preamp electronics which not only provide high spectral resolution in the hard X-ray and gamma-ray line energy range (10 keV to ≳10 Mev) but extend up to 250 MeV with good linearity. Thus the Ge detectors can be used as a primary detector of high energy neutrons and ≳10 MeV to 250 MeV gamma-rays. Used in a telescope configuration together with rear anti-coincidence shield crystals, the Ge detectors should be able to identify and separate high energy neutrons from gamma-rays.

Laboratory and Flight Testing

For detector testing, single-site interactions are produced in the detector by forcing a single Compton scatter at 90° plus or minus 3° by collimation of both the incoming 1173 keV photons and outgoing scattered 356 keV photons (Figure 4). In addition, the energy losses in the germanium detectors are restricted to those values and coincidence is required. Under those conditions more than 95% of the 817 keV energy losses are single site.

Examples of actual germanium detector current pulses are shown in Figure 5 for single energy depositions at different radial distances, and in Figure 6 for multiple-site interactions at nearly the same energy (836 keV from ^{54}Mn). For the same time-to-peak the current peak height is generally lower for multiples than for singles. The distributions of singles and multiples are shown in Figure 7. The dashed line in each figure is drawn approximately through the centroids of the distribution of peak heights at each time-to-peak for the singles. Note that multiples generally tend to be below the dashed line.

These tests confirm the feasibility and usefulness of the pulse shape analysis for background rejection. Using just the distribution of peak height versus time-to-peak criteria, it is possible to reject ~90% of the singles while still collecting ~60% of the multiples. Clearly, much more information is present in the pulse shape for discriminating between singles and multiples. But even this crude two-parameter analysis gives very significant gains (~ a factor of 2) in effective sensitivity. More detailed discussion of the laboratory measurements is given in *Smith et al.* (1988).

A test flight of a single two-segmented Ge detector in a thick CsI shield and NaI Collimator was carried out in March 1988 which verified the background rejection capabilities of this system. In this test flight, the laboratory (LeCroy) electronics system (Figure 3) was flown and the pulse shape telemetered down to the ground.

III. Position Sensitive Germanium Detectors

The hard X-ray imaging observations from SMM were of fundamental importance in that they provided direct evidence for non-thermal electron beams. Because of the low sensitivity of the HXIS instrument, only a very few intense flares were observed which could be imaged in hard X-rays. The HXIS energy range extended up to 30 keV, and it is possible that after the initial impulsive spike the images were dominated by the hot isothermal component (*Lin et al.*, 1981). This may be the reason that the 16–30 keV images later in the flare showed brightening at the top of the flare loop.

The hard X-ray foot point brightenings contrast with the VLA images of microwave brightenings at the tops of flare loops. Microwave emission is believed due to gyro-synchrotron emission of $\gtrsim$0.1 MeV electrons. It is of fundamental importance to the physics of flare particle acceleration to resolve this X-ray/microwave difference. Are the high energy electrons somehow accelerated and trapped at the tops of the loops, while the low energy electrons are beamed downward? Or are we seeing the effects of microwave emission and absorption processes? Clearly, imaging at 30 to >100 keV energies is very important. Furthermore, much higher sensitivity is needed, both to observe a wide range of flare intensities, and in the hope of determining not just the main electron collisional loss site but also the electron acceleration site.

At present, studies are progressing on much larger and quite novel hard X-ray imaging instruments, the gamma-ray and hard X-ray imaging (GRID) instrument for the MAX'91 Solar Balloon Program, spacecraft, and the Pinhole-Occulter Facility (P/OF), which hopefully will be flown on the Space Shuttle, and eventually, on the Advanced Solar Observatory (*Dabbs et al.*, 1982).

As presently envisioned the P/OF instruments would depend primarily on the Fourier transform imaging technique to obtain high angular resolution (see Figure 8). Two widely spaced, fine-scale grids create a large-scale modulation pattern of high-energy photons which can be measured by a detector with only moderate spatial resolution. This modulation pattern contains the phase and amplitude information for a single Fourier component of the source distribution. Each pair of grids, therefore, provides information analogous to a single "baseline" in radio interferometry. The GRID or P/OF instruments use multiple grid pairs with a variety of slit spacings and angular orientations to sample numerous Fourier components. An image is constructed from these Fourier components in exact analogy to image formation using multi-baseline radio interferometers such as the VLA.

NaI scintillation detectors used as Anger cameras can provide the required one-dimensional position information at energies from ~100 keV to the MeV region, but these detectors have poor position resolution at lower energies. Conventional position sensitive xenon proportional counters operated at 1 or 2 atmospheres pressure are inherently limited in spatial resolution by the path

length of photoelectrons in the gas (~1 cm at 50 keV and 1 atmosphere), and perhaps more important, provide insufficient stopping power to reach energies of 10^2 keV for practical detector thicknesses.

Under this grant, we investigated three very promising approaches for hard X-ray imaging detectors which can provide good to excellent stopping power up to >150 keV, and spatial resolution of from a few to a few tenths of mm. In addition these three approaches provide much better energy resolution than obtainable with NaI scintillation detectors or xenon proportional counters. The three approaches are:

1) Position-sensitive germanium "drift chamber," where the germanium charge pulse is drifted in a small electric field and its transit time is a function of distance along one dimension. A laboratory prototype has been fabricated and 1-D spatial resolution of ~0.5 mm achieved for 60 keV X-rays (see *Luke et al.*, 1985).

2) Position-sensitive germanium detectors where the current pulse shape is used to give the position in one dimension. This technique is based on work with pulse shape analysis for background reduction (see section I, Figure 5) in coaxial detectors.

3) High pressure (10–40 atmospheres) xenon gas scintillation drift chambers which, in principle, could give 3-D location by a combination of drift plus 2-D readout. A small (~10 cm dia) laboratory version has been fabricated and tested under a CalSpace grant. This technique is adaptable to large area detectors, and may provide response down to low, $\lesssim$5 keV energies. This last detector is described in section III.

Germanium Drift Chambers

A Ge drift chamber has been fabricated recently by the LBL detector group (see *Luke et al.*, 1985, in Appendix C, for details). The detector consists of a planar 3cm×3cm×0.3cm thick piece of Ge with p^+ contacts on both planar sides and an n^+ contact at the center of one end (Figure 9). The impurity concentration has a gradient from the n^+ contact to the other end. As voltage is applied the detector depletes from the two planar sides toward the middle, reaching full depletion first at the end opposite the n^+ contact. When sufficient voltage is applied so the detector depletes fully everywhere, a transverse drift field is set up along the central plane of the detector. The electrons of the electron-hole pairs created by energy depositions in the detector initially drift rapidly toward this center plane, while the holes drift to the p^+ contacts. Current pulses are thus produced on the p^+ contacts. Once the electrons reach the center plane they drift slowly in the transverse field toward the n^+ contact, producing a pulse when they reach the contact. The timing between the n^+ contact pulse and the p^+ contact pulses gives the spatial location in one dimension. Spatial resolution of ~0.5 mm has been obtained for 60 keV X-rays.

We have evaluated this type of detector. Trapping in the detector gives non-uniform spatial and spectral response, so careful mapping is required to maintain good energy resolution over the entire detector. Operation at somewhat elevated temperatures can help by reducing trapping. We find that the spectral resolution of the detector taken as a whole is poor (~6 keV FWHM, see Figure 10), but that the resolution at a given location is much better, typically 1–3 keV FWHM at the ^{241}Am 60 keV line. Thus by keeping track of the location (which would be done anyway to spatially resolve the source), and correcting for gain variations with location (Figure 11), an effective spectral resolution of 1–3 keV FWHM can be achieved. Thus spatial resolution of ~1 mm and spectral resolution of a few keV can routinely be obtained in a 3 cm × 3 cm detector.

Thick Planar Ge Detectors with Pulse Shape Analysis

As we and others (*Strauss and Sherman*, 1972) have shown, the shape of the current pulse collected from an energy deposition in a coaxial germanium detector depends on the location of the deposition (see Figure 5). We believe that a ~5 cm thick planar detector of the geometry shown in Figure 12 can be fabricated by using the very high purity material around the transition from *n* to *p* type impurities in germanium crystals. Such a detector could provide fairly uniform one-dimensional spatial resolution of ~1–2 mm, using refinements of the pulse shape techniques we have already developed. This type of detector may also be adapted for position sensing at gamma-ray energies, since the detector diameter of ~6 cm would provide the stopping power of a large coaxial Ge detector. Segmentation of the detector (dotted line in Figure 12) may help to separate the initial Compton scatter from subsequent interactions.

We have fabricated and tested a 3 cm thick planar germanium detector and developed our present pulse shape analysis techniques for position sensing in this detector.

Figure 13 shows a computer simulation of the current pulses from different locations in a thick planar detector. Pulse shape measurements on the 3 cm thick planar are in agreement with these simulations. Spatial resolution of a few mm appears feasible.

IV. High Pressure Xenon Gas Scintillation Drift Chambers

Together with Professor Sadoulet, we have been developing a high pressure xenon gas scintillation drift chamber, similar to the so-called "time projection chamber" or "imaging" chambers used successfully in particle physics, for use in hard X-ray and gamma-ray astronomy. In such a system (Figure 14), the gas of the chamber would be the converter, and the extracted electrons would be transported by an electric field towards a suitable bi-dimensional sensing plane which would give, by combination of the drift time and of the cell number, the original spatial coordinates. In that way, an image of the full interaction would be obtained with a pixel size on the order of a millimeter in the 3 dimensions. The energies involved in each event would also be measured by pulse height.

The extracted electrons are detected via gas scintillation (*Sims et al.*, 1984 and references therein), with a novel read-out technique on the use of wave-shifter fibers (*Garwin*, 1960; *Eckardt et al.*, 1978; *Fent et al.*, 1984). Gas scintillation relies on the emission of UV light when the electrons extracted by the original interaction drift into a strong electric field. The medium is transparent to this light. This light is then wave-shifted, sent along the optical fibers, and sensed by phototubes. Since many photons are produced, even a relatively poor collection efficiency leads to a few photoelectrons per initial electron.

The use of wave shifter fibers provides an elegant way of extracting the light, well adapted to the use of high pressure. Two-dimensional read-out can be implemented by allowing half of the light to go through the first layer and be collected by another layer at 90 degrees. The time of occurrence of the photon interaction can be obtained from the primary scintillation (from the initially produced photoelectrons and Compton electrons) of the gas. This will provide a time zero for the drift measurement.

The technological problems encountered in this new technique do not appear insurmountable. Basically, they are of three types.

1) Gas purity. Impurities will quench both the primary scintillation, and the secondary scintillation in the high field gap. Shortly, testing of the outgassing properties of many materials will begin.

2) Relatively high voltages. The present prototype, for instance, requires 60 kV but very small currents. However, proper engineering and production of high voltage directly in the chamber allows us to minimize potential problems.

3) High pressure. The detector is designed to operate at the maximum practical pressure with xenon of 40 atmospheres. This is not a great inconvenience if spherical shapes and modern composite materials can be used in order to minimize the amount of material. For instance, 1 gram/cm^2 of Kevlar-Epoxy is sufficient to hold 40 atmospheres with a radius of 50 cm and a safety factor of 10! Moreover, for work at lower energy, smaller pressures (10 atmospheres) would allow an even thinner window.

Such a technique has many potential advantages with respect to currently used techniques. In the region between 35 keV and 100 keV, such gas scintillation chambers offer an interesting alternative to xenon multiwire chambers. Contrary to the latter, they are easy to operate at large pressures, offering the possibility of large stopping power. In contrast to the usual avalanche detection method plagued by space charge effects and large fluctuation, gas scintillation energy resolution is completely dominated by the fluctuation in the number of extracted electrons, and resolution only about 3 times worse than that for germanium has been achieved. Large areas can be instrumented at much smaller cost than germanium detectors. There is also the possibility of

detecting the escape photons (emitted in 85% of the photoelectric effects) in xenon (*Sims et al.*, 1983), which will provide a powerful method of background rejection against neutron scattering, β-decays and Compton scattering of gamma-rays leaking through the shield (*Gehrels*, 1985).

A small prototype of a gas scintillation drift chamber has been built in Berkeley with funds provided by CalSpace, NASA Innovative Research, and the Lawrence Berkeley Laboratory. Figure 15 shows the chamber in its first configuration, where the light is observed through a quartz window by a set of 17 phototubes in an Anger camera geometry. Table II gives some of the chamber characteristics. Figure 16 shows some of the components of this detector.

Table II. Chamber Characteristics

I. Anger camera configuration	
Chamber diameter	6 cm
Drift length	7.1 cm
Scintillation gap	0.5 cm
Maximum working pressure	40 Atmospheres
Typical voltage settings (40 Atmospheres)	
Drift voltage	10 kV
Scintillation gap voltage	50 kV
Expected performance (pure xenon, 40 Atm)	
Number of UV photons/Initial electron	2200
Drift velocity (35 V/cm/atm)	10^5 cm/s
Total drift time	70 μs
II. Read-out by wave shifter fibers	
Diameter of fibers	0.1 cm
Theoretical maximum collection efficiency (number photo-electrons/number of UV photons)	0.25%

We have been operating this prototype for a year and a half. We have solved the problem of oxygen contamination we had at the beginning. We have connected the 16 phototubes reading out the chamber to a computer, providing approximately 50000 digitizings per event. This allowed us to demonstrate the imaging capability of our device. For instance, the time profile of X-ray pulses readily displays the presence of 2 pulses in case of emission of a K shell escape photon. The double pulse K shell signature is also observed in the wave shifter fiber read-out. This showed also that the individual X-ray pulses are simple enough to allow an on-board algorithm to summarize the information.

Most importantly, we have *demonstrated for the first time the operation of the wave-shifter read out.* Figure 17 shows our first uncorrected ^{241}Am spectrum obtained with fibers. The light collection efficiency of the fibers in a real chamber environment is observed with X-ray pulses to be $(2 \pm 0.5) \times 10^{-3}$ photoelectrons/initial UV photon light when the theoretical maximum is 3.2×10^{-3}. This is much higher than our conservative design estimate of 0.6×10^{-3}. The relatively large spatial spread of the light pulses that we observed is now understood and can be corrected.

The pattern of the pulses observed on the fibers which are grouped in strips of 8 mm clearly demonstrates the possibility of measurement of the xy position.

There is some degradation of the gas with fibers and without recirculation leading to a decrease of the pulse height of 20% per day. However, we have shown that passing the gas through a molecular sieve improves the light yield and our chamber has been able to work for 50 days with the same gas and with recirculation we could restore the initial pulse level. Therefore with a proper recirculation system this contamination should not be a problem.

Recently, we encountered a major difficulty when we discovered that the fibers were absorbing the gas and lengthening by about 3%. The fibers then bend and the spatial accuracy is compromised. This can be corrected by isolating the fibers from the gas, using thin quartz tubes.

We have begun the design of a large prototype gas scintillation chamber for solar hard X-ray imaging in the $\lesssim$5 keV to $\gtrsim$150 keV range. For applications to solar imaging instruments such as P/OF where Fourier transform grids would be used, only one-dimensional spatial resolution of $\lesssim$0.5 cm is required. Also 1 g/cm^2 column depth of xenon would provide 86% absorption at 80 keV photons and 50% at 150 keV. Such requirements are well within the capabilities of these detectors. Figure 18 shows a conceptual design for a solar hard X-ray Fourier transform imaging detector. This detector is operated at 10 atmospheres pressure and 18 cm depth for a total column depth of ~1.06 g/cm^2. The detector is large enough to provide room for at least 6–7 Fourier grid subcollimators. Two sets of orthogonal wavelength shifters will be used to provide the required spatial resolution for any orientation of the Fourier subcollimators. Fiberglass shells of the required size and shape have been fabricated and tested to 20 atmospheres.

V. Long Duration Balloon Flights for Solar High Energy Observations

The ideal platform for high energy solar measurements would permit continuous coverage of the Sun over the $\gtrsim$5-year duration of the solar maximum. Such a platform could be provided by a spacecraft in heliocentric orbit, located at the Lagrange point L_1 between the Sun and the Earth. It is important to note, however, that high energy, $\gtrsim$15 keV measurements, can be obtained from high altitude balloons, and that it is now possible to obtain long duration, $\gtrsim$1-month, balloon flights by circumnavigating the globe. In 1982 a 15 million cu ft balloon with an ~1200 lb payload made a circumnavigation of the globe in the southern hemisphere. The balloon was a standard zero pressure balloon operated in the RAdiation COntrolled balloON mode (RACOON). The main characteristic of RACOON long duration flight are:

1) The balloon is at high altitude during sunlit hours but drops during nighttime, making RACOON particularly suitable for solar observations.

2) Thus, essentially ~12 hours of continuous high altitude observations are obtained each day. This contrasts with typical low altitude spacecraft (such as SMM), which have an ~2-hour orbit with ~40 minutes Earth shadow each orbit. Very often the start or decay phase of a large flare would be missed. Coverage through an entire flare including at least $\sim 10^3$ s after the impulsive phase is important to obtain the delayed emissions from positron annihilation, neutrons, etc. Furthermore, it may be possible to obtain ~24-hour coverage at high energies with flights over Antarctica during its summer.

3) The energetic particle radiation environment is much less severe at balloon altitudes than on low orbiting spacecraft. This is important to minimize both radiation damage to the detectors and electronics, and activation of the detector in the South Atlantic anomaly.

4) It is much easier and cheaper to provide cryogenic cooling on balloons than on spacecraft. Normal liquid nitrogen dewars are used in balloons, but extremely expensive and complex solid cryogen or mechanical coolers are required for spacecraft, because of the weightless environment in orbit.

5) Because of the much more benign launch environment and the capability for repairs after each flight, balloon experiments need not be designed to space-qualified specifications. These are usually major cost drivers for (space) experiments.

6) The currently available resources on a RACOON long duration balloon flight – ~50 watts from solar cells, and ~60 bits per s data rate over ~2/3 of the globe through GOES, METEOSAT, and TRANSIT – are already sufficient for simple spectroscopic studies of solar flares and other transients.

7) At present, around-the-world flights are possible only in the southern hemisphere, for political reasons. Since the winds are favorable only in the local summer, a season of ~3 months (Dec.-Feb.) is available. However, long duration flights from the U.S. to Japan and China should also be investigated. These should provide ~5–7 day long flights.

The reliability of LDBF needs to be established, and the resources available (weight, power, telemetry rate) should be expanded in the next few years. It appears to us that LDBF can provide a platform for high energy solar physics which may be highly advantageous, especially in terms of cost.

We have developed, fabricated, tested, and flown an LDBF payload carrying an array of planar germanium detectors (50 cm^2 area) and an array of large area (700 cm^2 total) phoswich NaI/CsI scintillation detectors for high sensitivity observations of solar hard X-ray microflares (see Figure 1 of Appendix B). The launch of this payload, originally planned for Jan.–Feb. 1985 was postponed to Jan.–Feb. 1986 due to diplomatic problems with obtaining an official U.S.-Australian agreement on such flights. It was postponed from 1986 to 1987 because of the moratorium on all

balloon flights which was imposed after the disastrous rash of balloon failures in the fall 1985 domestic campaign. This payload was launched on February 9, 1987, from Alice Springs, Australia, and successfully flew for 12 days before being cut down in Brazil on February 21. Appendix B provides a detailed description of the payload and of the flight performance.

A second long duration balloon flight was carried out in March 1988 with a single segmented coaxial germanium detector with pulse shape discrimination. Due to a failure in the power system only one day of data was obtained. These data, however, proved the feasibility of the pulse shape discrimination technique and provided the first measurement of β-decay background from cosmic ray activation of the detector. A description of the 1988 LDBF is given in Appendix C.

We have also made a preliminary study of the possibilities for Antarctic long duration balloon flights for solar observations. The results are summarized in Appendix D.

VI. Bibliography

The following papers, copies of which are provided with this report, have resulted from research supported by this grant:

1. Dennis, B., R. Canfield, M. Bruner, G. Emslie, E. Hildner, H. Hudson, G. Hurford, R. Lin, R. Novick and T. Tarbell, MAX '91: Flare research at the next solar maximum, 52 pp., NASA, Washington, D.C., 1988.
2. Gehrels, N., C. Crannell, D. Forrest, R. Lin, L. Orwig and R. Starr, Hard X-ray and low-energy gamma-ray spectrometers, *Solar Phys.* **118**, 233, 1988.
3. Levedahl, W. K., Effect of wave localization on plasma instabilities, Ph.D. Dissertation, Physics Department, University of California, Berkeley, 1987.
4. Lin, R., D. Curtis, J. Primbsch, P. Harvey, W. Levedahl, D. Smith, R. Pelling, F. Duttweiler and K. Hurley, A long-duration balloon payload for hard X-ray and gamma-ray observations of the sun, in *Recent Advances in the Understanding of Solar Flares: Proc. of the U.S.-Japan Seminar, April 1987*, ed. by H. Hudson and K. Kai, *Solar Phys.* **113**, 333, 1987.
5. Lin, R. P., A high resolution gamma-ray, hard X-ray, and neutron spectrometer for solar flare observations, in *Nuclear Spectroscopy of Astrophysical Sources, AIP Conf. Proc.* **170**, ed. by N. Gehrels and G. Share, p. 456, Amer. Inst. of Physics, New York, 1988.
6. Lin, R., D. Curtis, P. Harvey, K. Hurley, J. Primbsch, D. Smith, R. Pelling and F. Duttweiler, A high resolution gamma-ray and hard X-ray spectrometer for solar flare observations in Max-91, in *Max '91: Flare Research at the Next Solar Maximum*, ed. by R. C. Canfield, p. 262, NASA Goddard Space Flight Center, Greenbelt, MD, 1988.
7. Lin, R. P., Solar particle acceleration and propagation, *Rev. Geophys.* **25**, 676, 1987.
8. Parsons, A., B. Sadoulet, S. Weiss, D. Smith, K. Hurley, R. Lin and G. Smith, The gas scintillation drift chamber as a hard X-ray detector, in *Nuclear Spectroscopy of Astrophysical Sources, AIP Conf. Proc.* **170**, ed. by N. Gehrels and G. Share, p. 478, Amer. Inst. of Physics, New York, 1988.
9. Parsons, A., B. Sadoulet, S. Weiss, T. Edberg, J. Wilkerson, G. Smith, R. Lin and K. Hurley, High pressure gas scintillation drift chambers with wave shifter fiber readout, *IEEE Trans. Nucl. Sci.* **NS-36**, 931, 1989.

10. Sadoulet, B., R. P. Lin and S. C. Weiss, Gas scintillation drift chambers with wave shifter fiber read-out for hard X-ray astronomy, *IEEE Trans. Nucl. Sci.* **NS-34**, 52, 1987.

11. Sadoulet, B., S. Weiss, A. Parsons, R. Lin and G. Smith, Gas scintillation drift chambers with wave shifter fiber readout, *IEEE Trans. Nucl. Sci.* **NS-35**, 543, 1988.

References

Chupp, E. L., *Solar Phys., 86*, 383, 1983.

Chupp, E. L., D. J. Forrest, J. M. Ryan, J. Heslin, C. Reppin, K. Pinkau, G. Kambach, E. Rieger, and G. H. Share, *Astrophys. J. Lett., 263*, L95, 1982.

Dabbs, J. R., E. A. Tandberg-Hanssen, and H. S. Hudson, *NASA Tech. Paper 2089*, 1982.

Eckardt, V. *et al., Nucl. Instr. and Meth., 155*, 389, 1978.

Fenimore, E. L., J. G. Laros, R. W. Klebesadel, R. E. Stockdale, and S. R. Kane, in *Gamma Ray Transients and Related Astrophysical Phenomena*, ed. by R. E. Lingenfelter *et al.*, p. 201, AIP, New York, 1982.

Fent, A. *et al., Nucl. Instr. and Meth., 225*, 509, 1984.

Garwin, R. C., *Rev. Sci. Instr., 31*, 1010, 1960.

Gehrels, N., *Nucl. Inst. Meth., A239*, 324, 1985.

Hoyng, P., A. Duijveman, M. E. Machado, D. J. Rust, Z. Svestka, A. Boeless, C. de Jager, K. J. Frost, H. Lafleur, G. M. Simnett, H. F. van Beek, and B. E. Woodgate, *Astrophys. J. Lett., 246*, L155, 1981.

Lin, R. P., R. A. Schwartz, R. M. Pelling, and K. C. Hurley, *Astrophys. J. Lett., 251*, L109, 1981.

Lin, R. P., R. A. Schwartz, S. R. Kane, R. M. Pelling, and K. C. Hurley, *Astrophys. J., 283*, 421, 1984.

Lin, R. P., and R. A. Schwartz, *Astrophys. J., 312*, 462, 1987.

Lin, R. P., R. A. Schwartz, S. R. Kane, R. M. Pelling, and K. C. Hurley, *Astrophys. J., 283*, 421, 1984.

Luke, P. N., N. W. Madden, and F. S. Goulding, *IEEE Trans. Nucl. Sci., NS-32*, 457, 1985.

Luke, P. N., *ISEE Trans. Nucl. Sci., NS-31*, 1984.

Marsh, K., and G. J. Hurford, *Astrophys. J. Lett., 240*, L111, 1980.

Matteson, J. L., P. L. Nolan, W. S. Paciesas, and R. M. Pelling, *Space Sci. Instr., 3*, 491, 1977.

Murphy, R. J., R. Ramaty, D. J. Forrest, and B. Kozlovsky, in *19th Internat'l. Cosmic Ray Conf. Papers*, ed. by F. C. Jones *et al., NASA Conf. Publ. 2376*, vol. *4*, 249, 1985.

Pehl, R. H., *NASA Tech. Memorandum 79619*, 473, 1978.

Ramaty, R., in P. A. Sturrock, T. E. Holzer, D. Mihalas, and R. K. Ulrich (eds.), *The Physics of the Sun*, Vol. II, Chap. 14, D. Reidel Publ. Co., Dordrecht, Holland, p. 291, 1986.

Ramaty, R., B. Kozlovsky, and R. E. Lingenfelter, *Space Sci. Rev., 18*, 341, 1975.

Roth, J., J. H. Primbsch, and R. P. Lin, *IEEE Trans. Nucl. Sci., NS-31*, 367, 1984.

Sims, M. R., *Nucl. Instr. and Meth., 211*, 499, 1983.

Sims, M. R. *et al., Nucl. Instr. and Meth., 221*, 168, 1984.

Smith, D. M., M. Shapshak, R. Campbell, J. H. Primbsch, R. P. Lin, P. N. Luke, N. W. Madden, and R. H. Pehl, in *Nuclear Spectroscopy of Astrophysical Sources*, N. Gehrels and G. H. Share (eds.), Amer. Inst. Phys., New York, p. 484, 1988.

Strauss, M. G., and I. S. Sherman, *IEEE Trans. Nucl. Sci., NS-19*, 219, 1972.

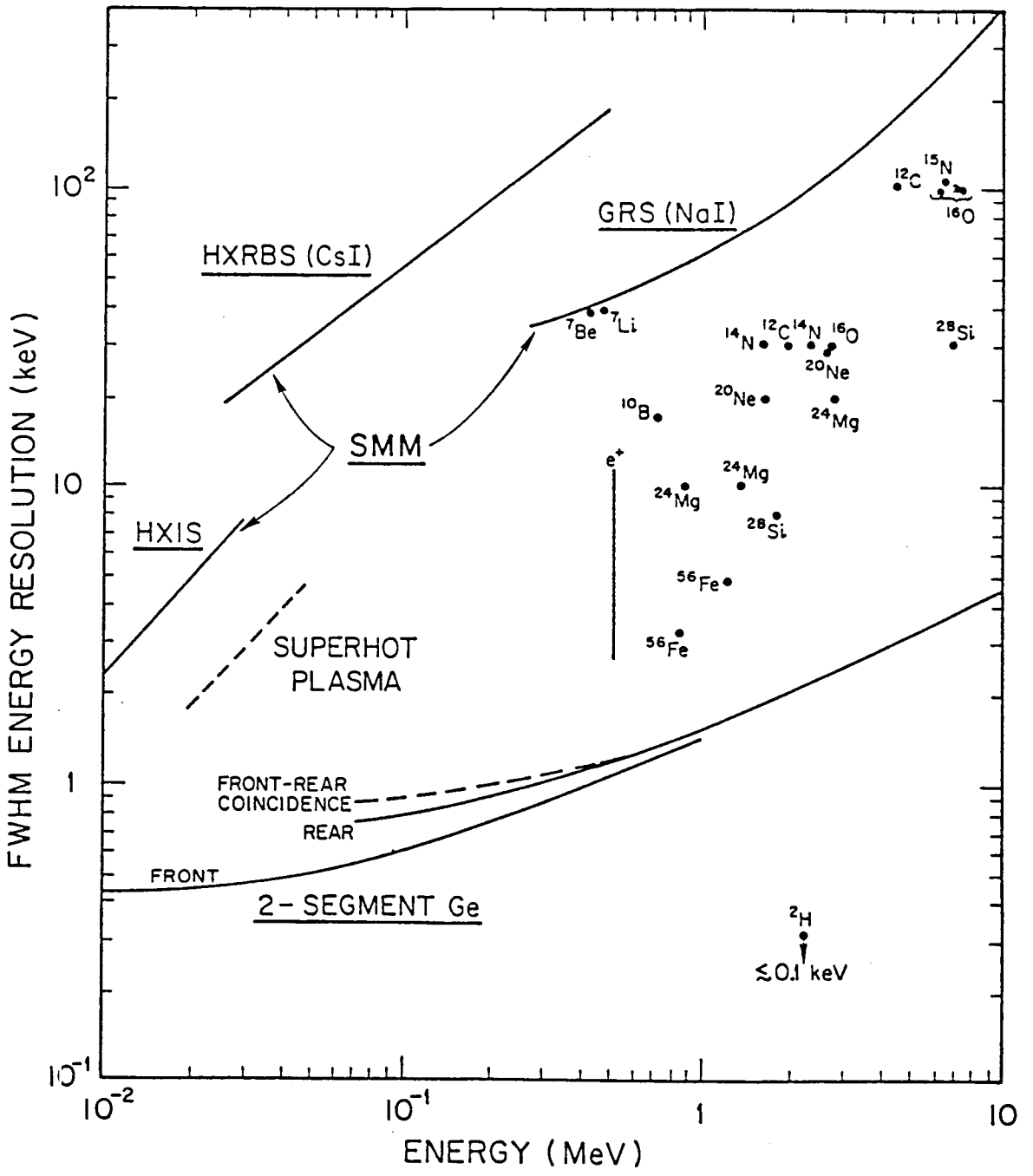

Figure 1. The FWHM energy resolution of the hard X-ray and gamma-ray detectors on SMM plotted as a function of the photon energy for comparison with the resolution of cooled, high-purity, germanium detectors. Also shown are the predicted widths of the gamma-ray lines expected in solar flares and the resolution required to resolve the extremely steep spectrum of the superhot plasma.

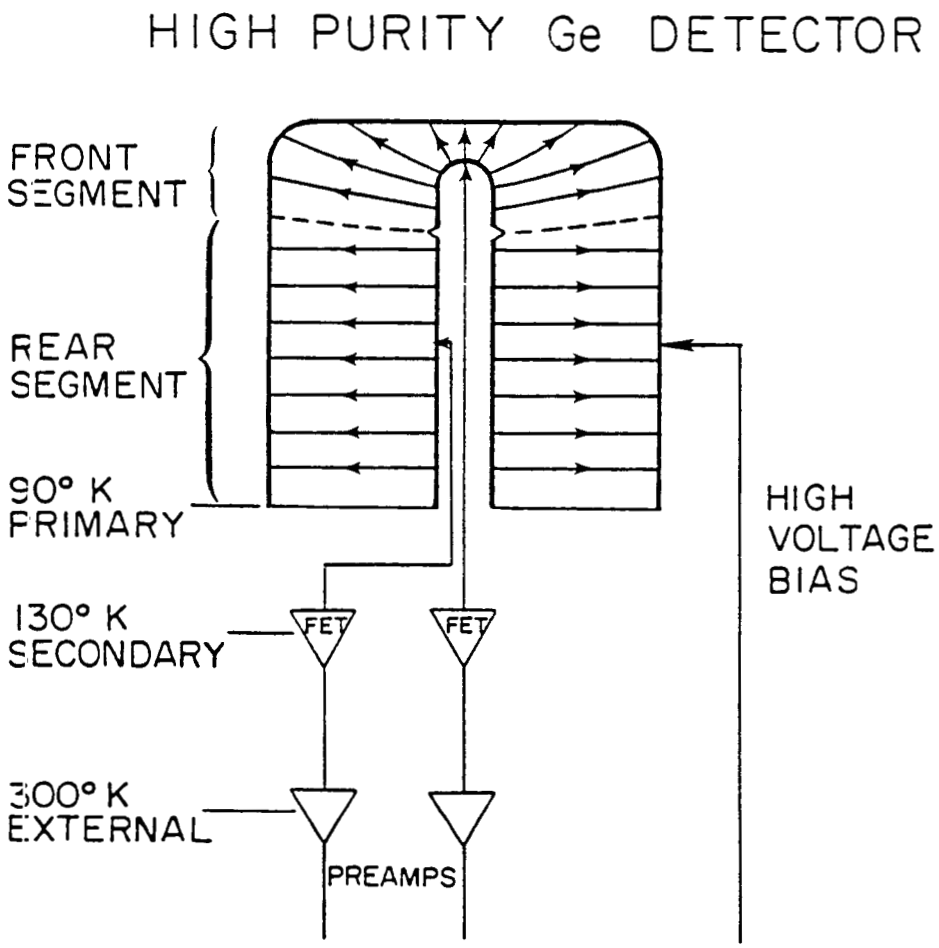

Figure 2. Concept of a segmented HPGe detector.

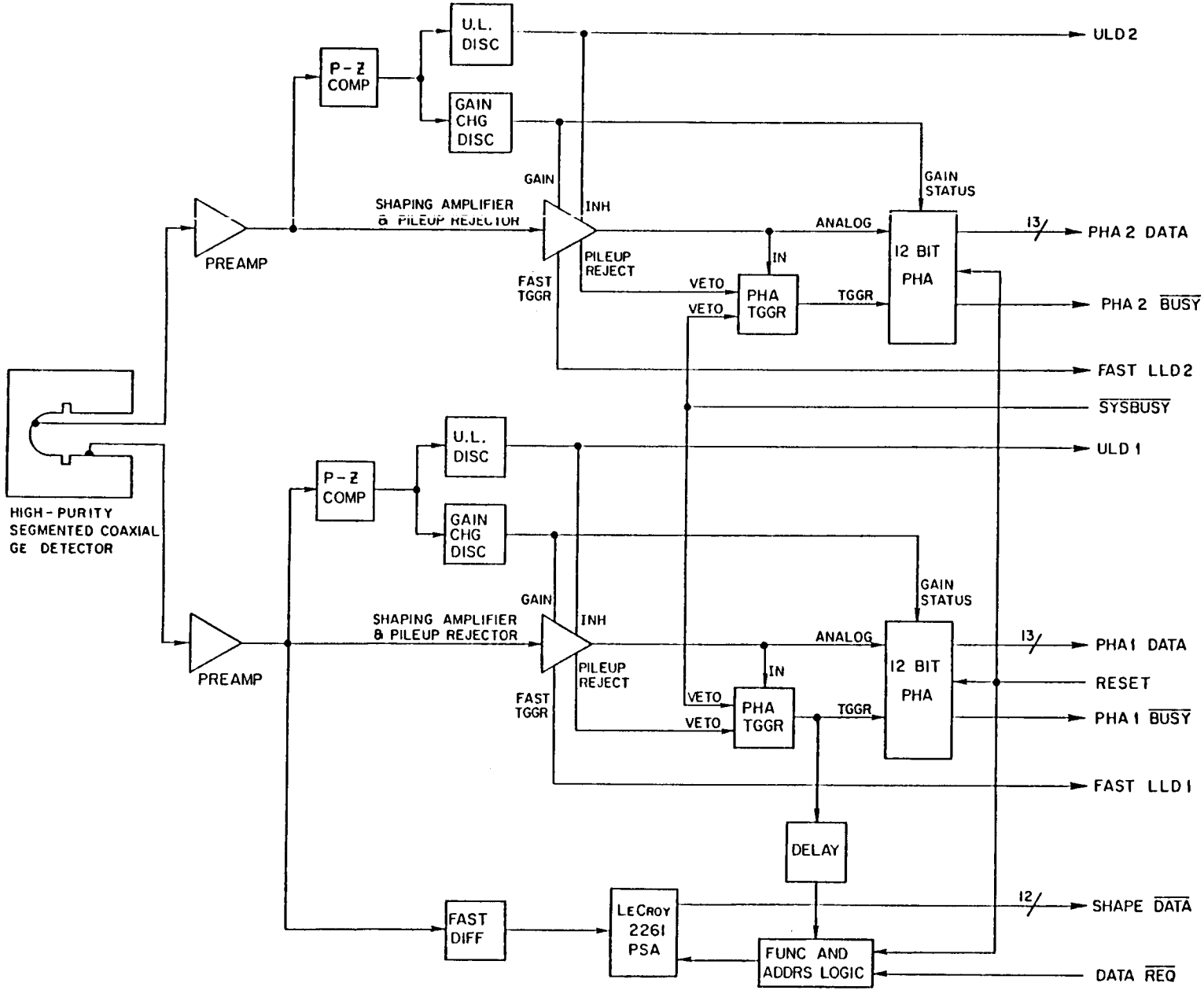

Figure 3. SEGMENTED DETECTOR FLIGHT ELECTRONICS

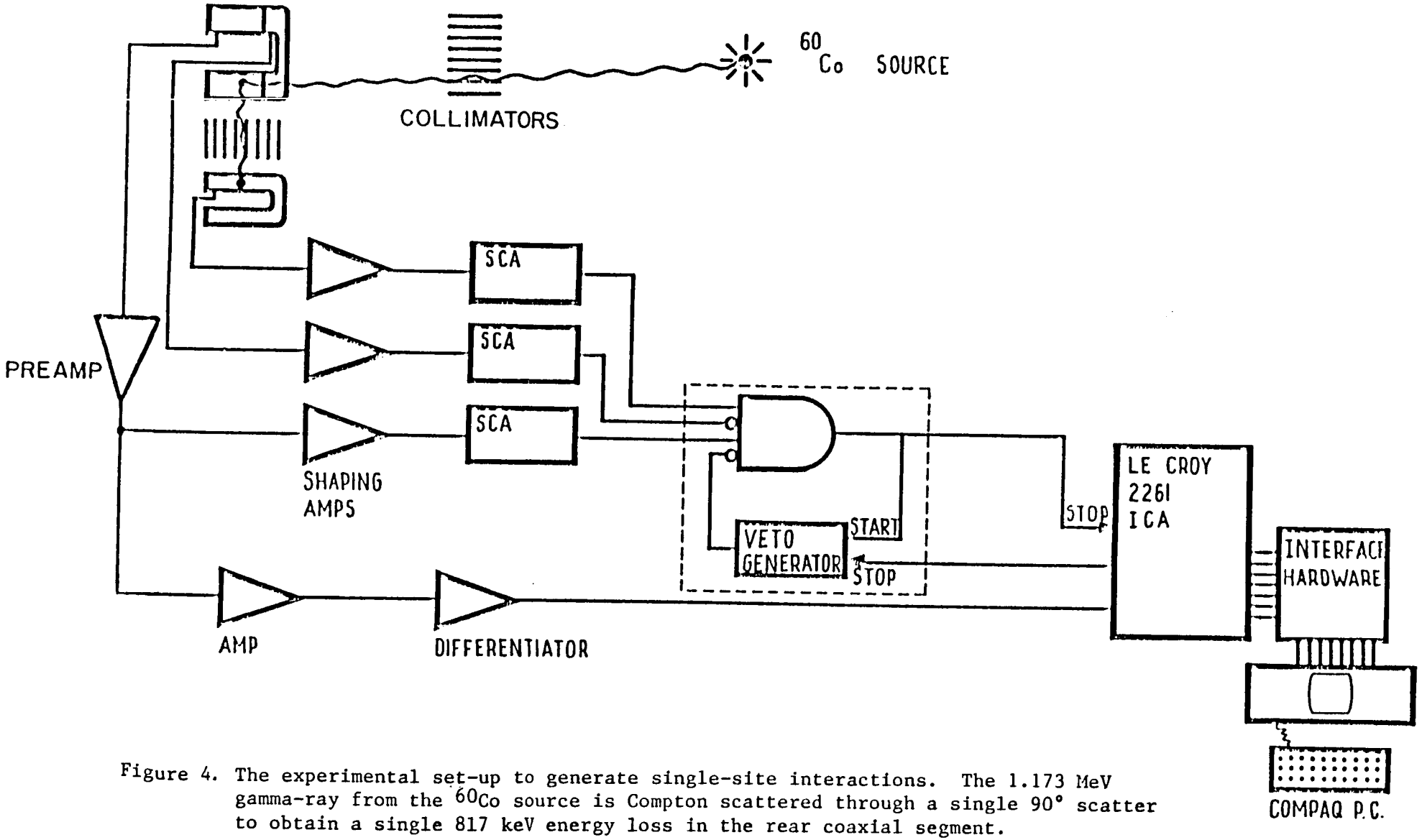

Figure 4. The experimental set-up to generate single-site interactions. The 1.173 MeV gamma-ray from the ^{60}Co source is Compton scattered through a single 90° scatter to obtain a single 817 keV energy loss in the rear coaxial segment.

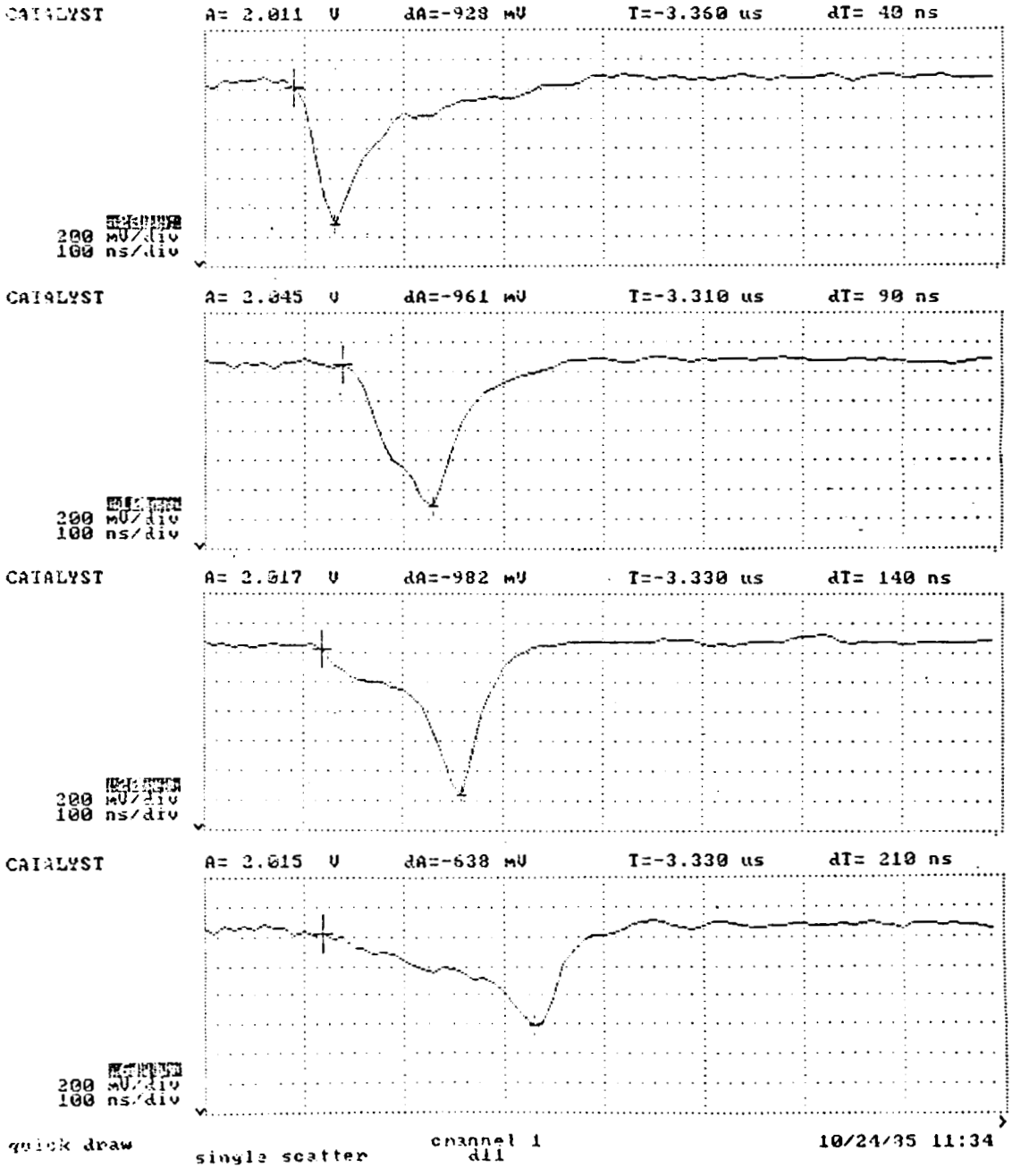

Figure 5. Current pulse shapes obtained for 817 keV single site interactions, ranging from interactions near the central electrode (top) to the outer edge (bottom) of the detector.

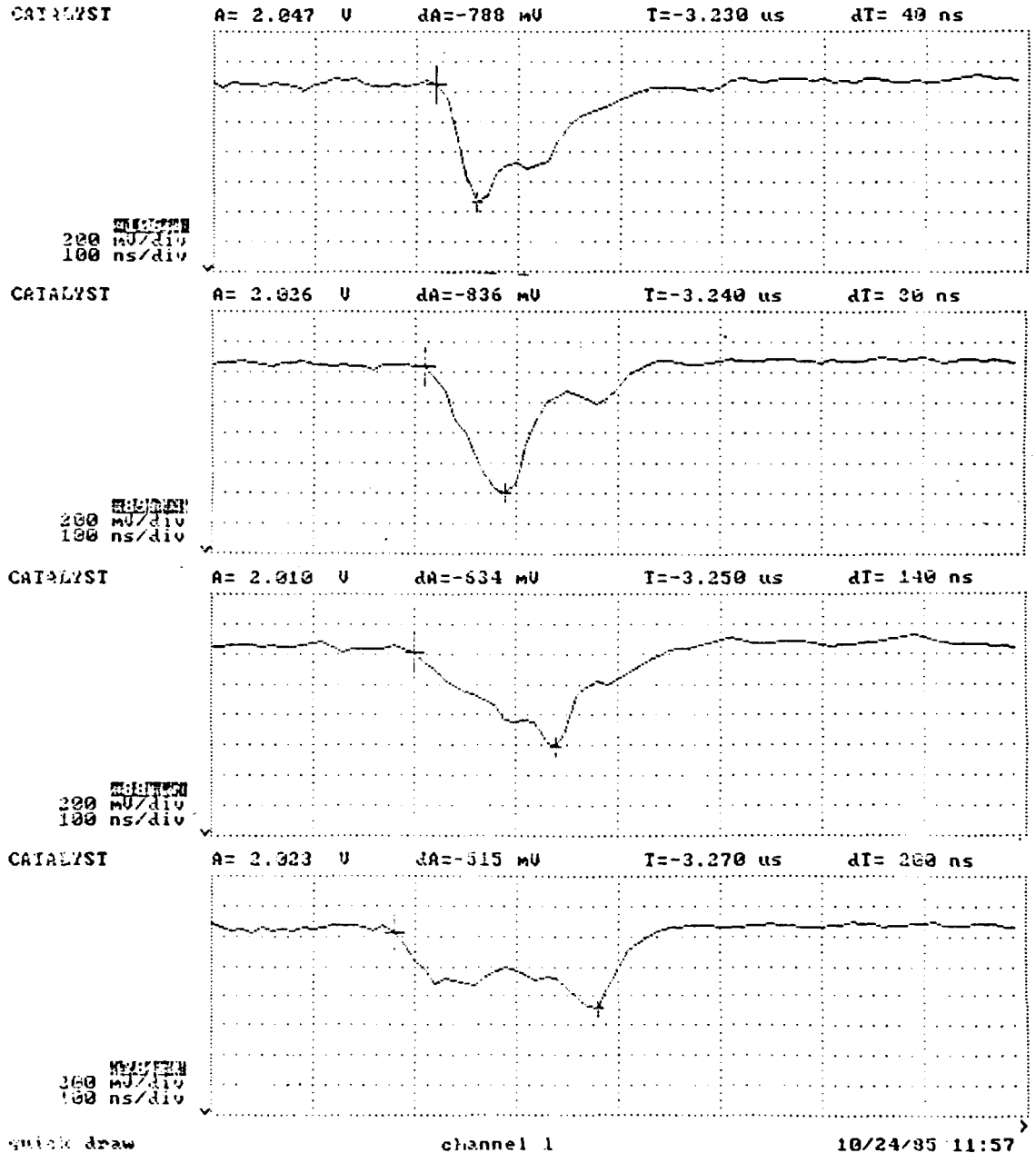

Figure 6. Current pulse shapes obtained for 835 keV multiple site interactions (^{54}Mn source) for comparison at about the same time to peak. Note the peak height is generally lower.

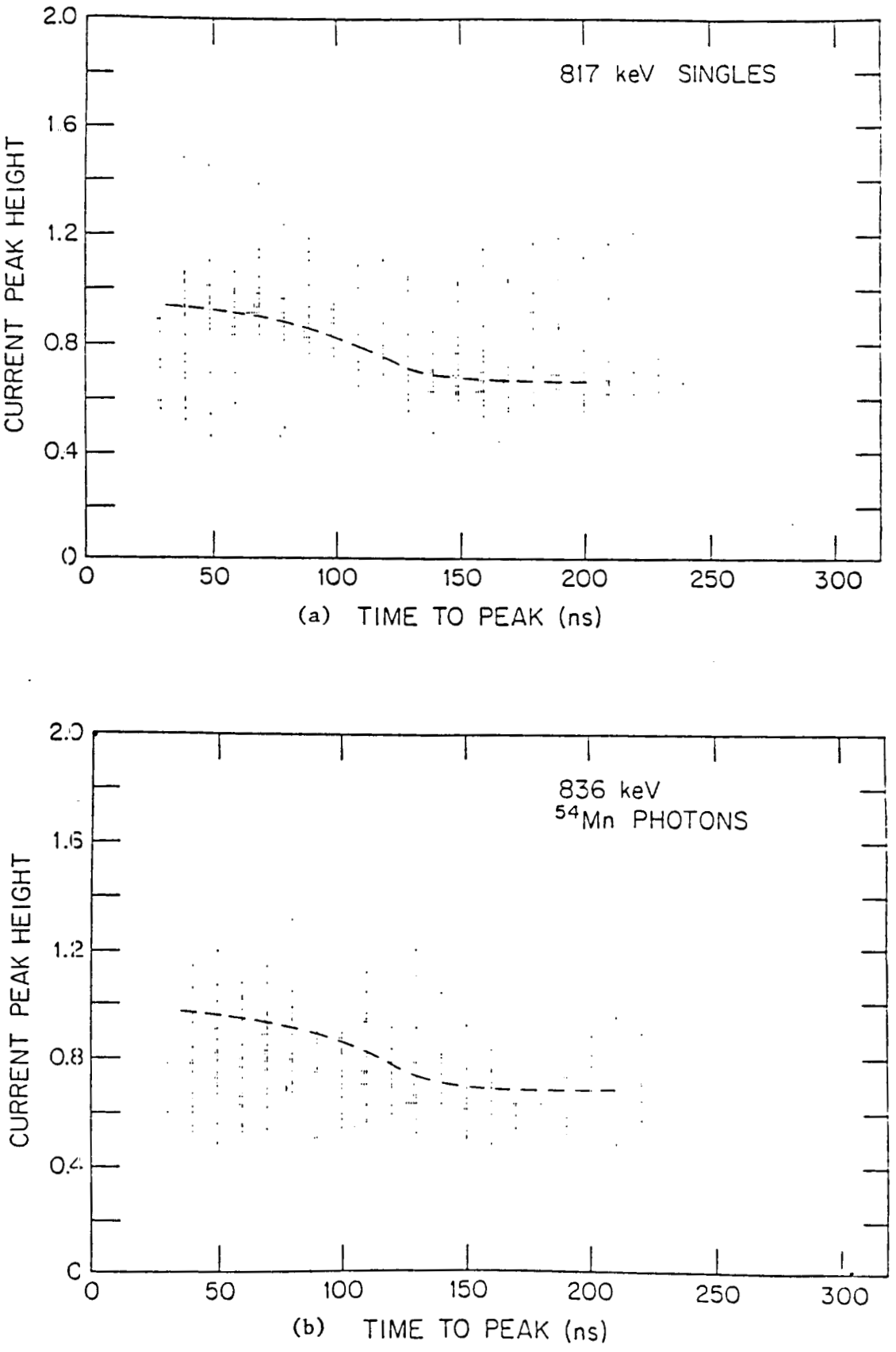

Figure 7. Distribution in peak height versus time to peak. (a) singles. (b) multiples.

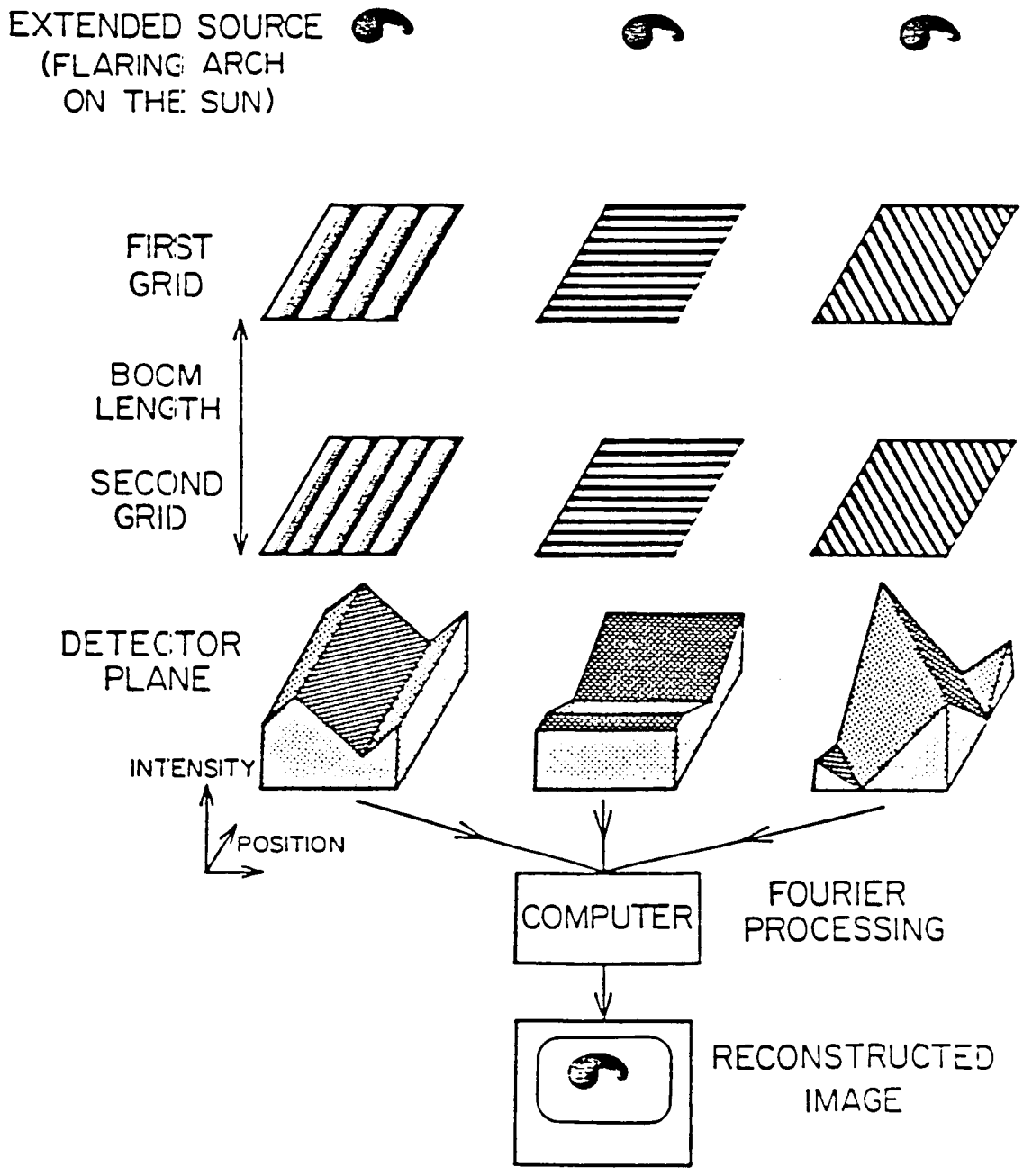

Figure 8. A Schematic illustration of the Fourier-Transform imaging technique. (see Hurford and Hudson, 1979, for details)

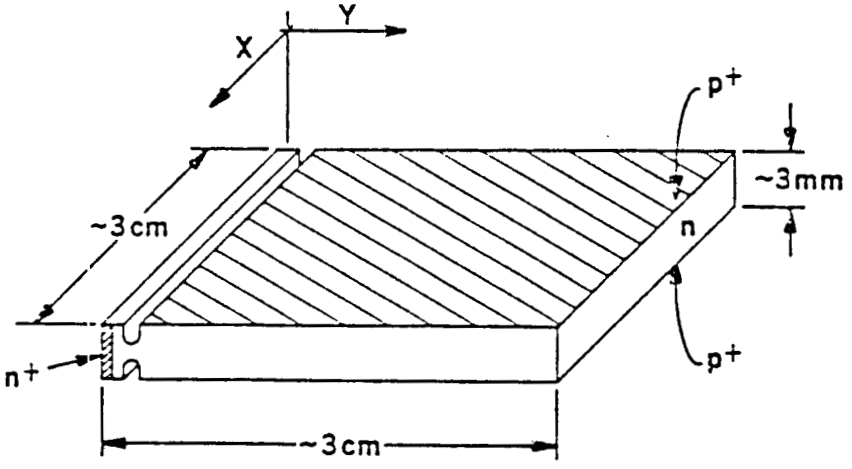

Figure 9. Structure and approximate dimensions of the germanium drift chamber.

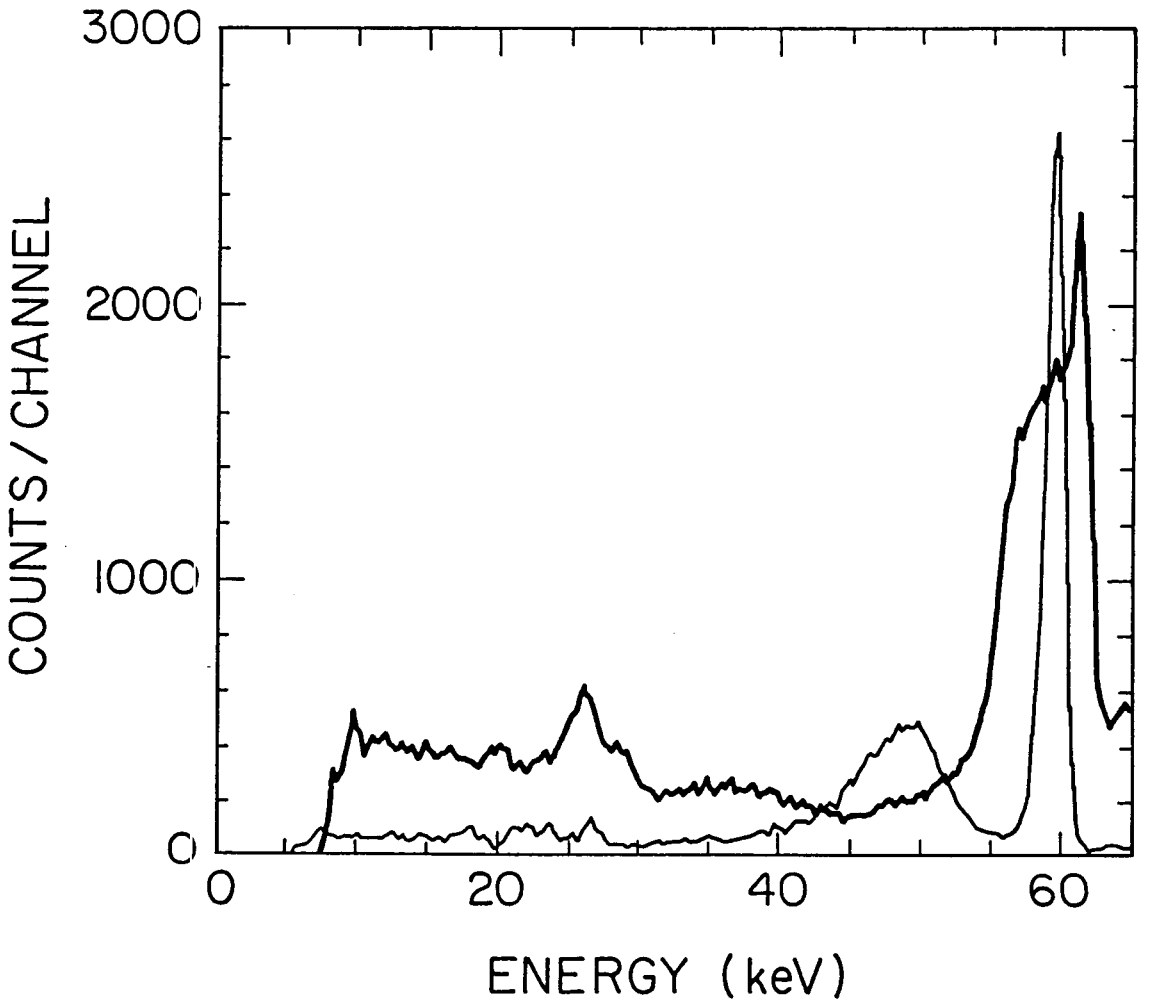

Figure 10. Spectrum of ^{241}Am taken over the whole detector (thick line) and at a single location (thin line).

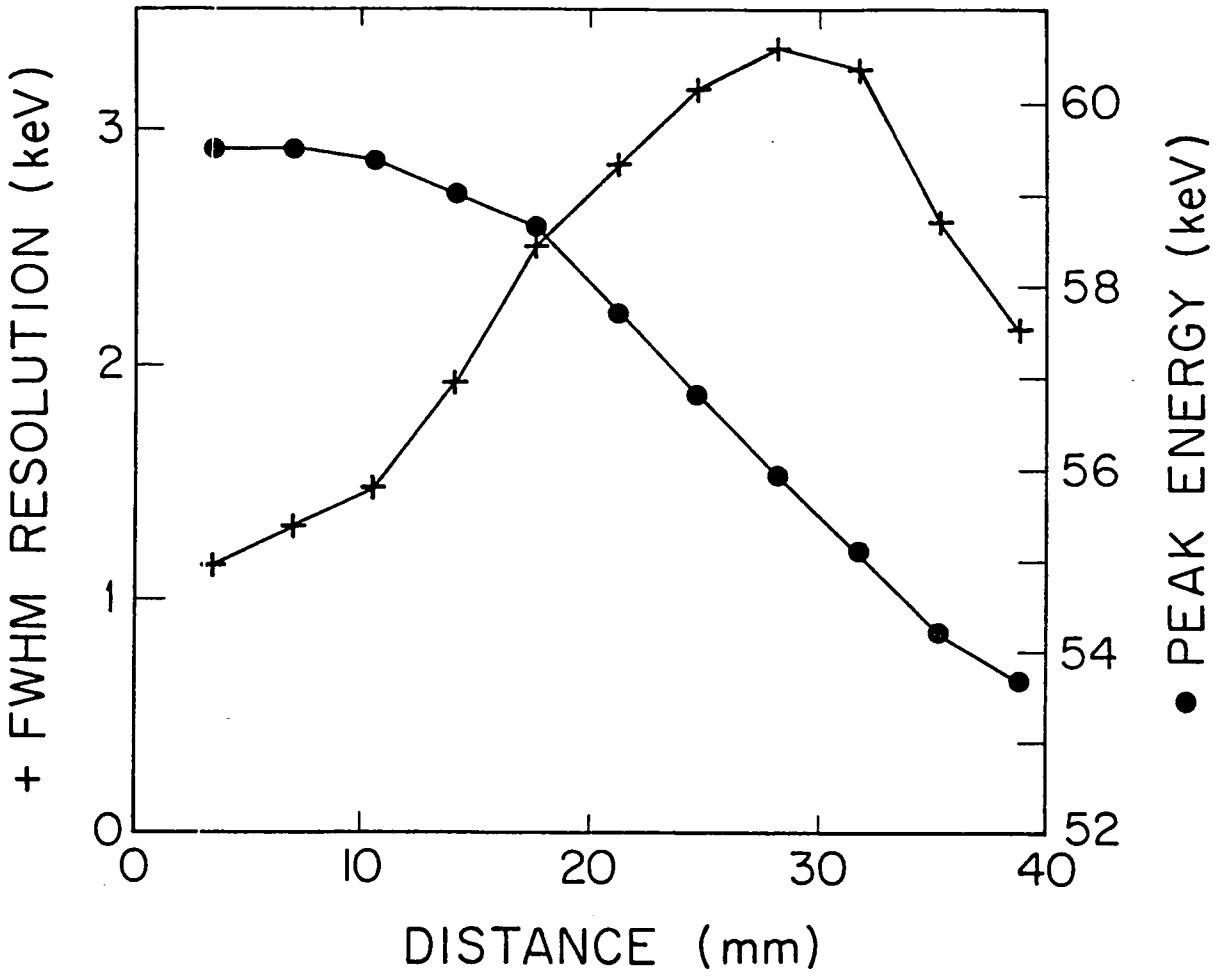

Figure 11. The FWHM spectral resolution (crosses) and the center energy of the ^{241}Am 60 keV peak (dots) are plotted here as a function of distance along the detector.

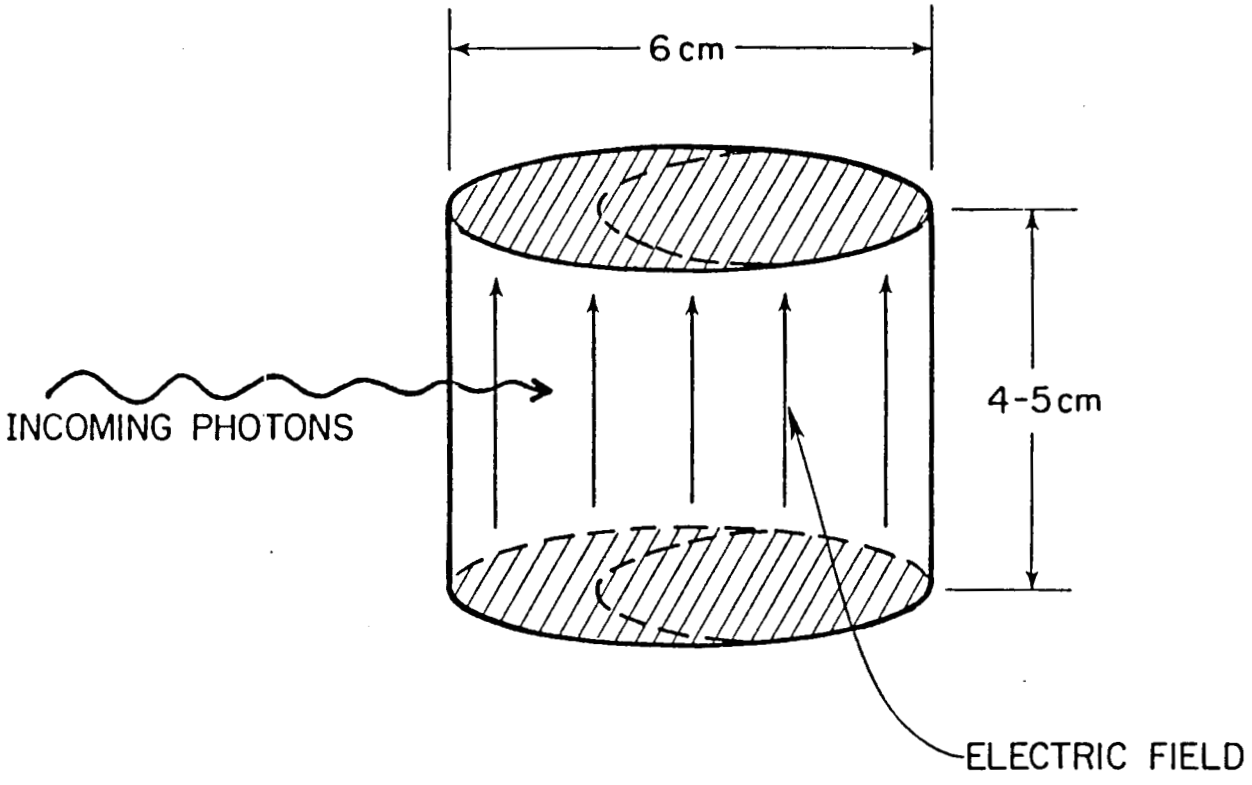

Figure 12. Schematic of a thick planar detector.

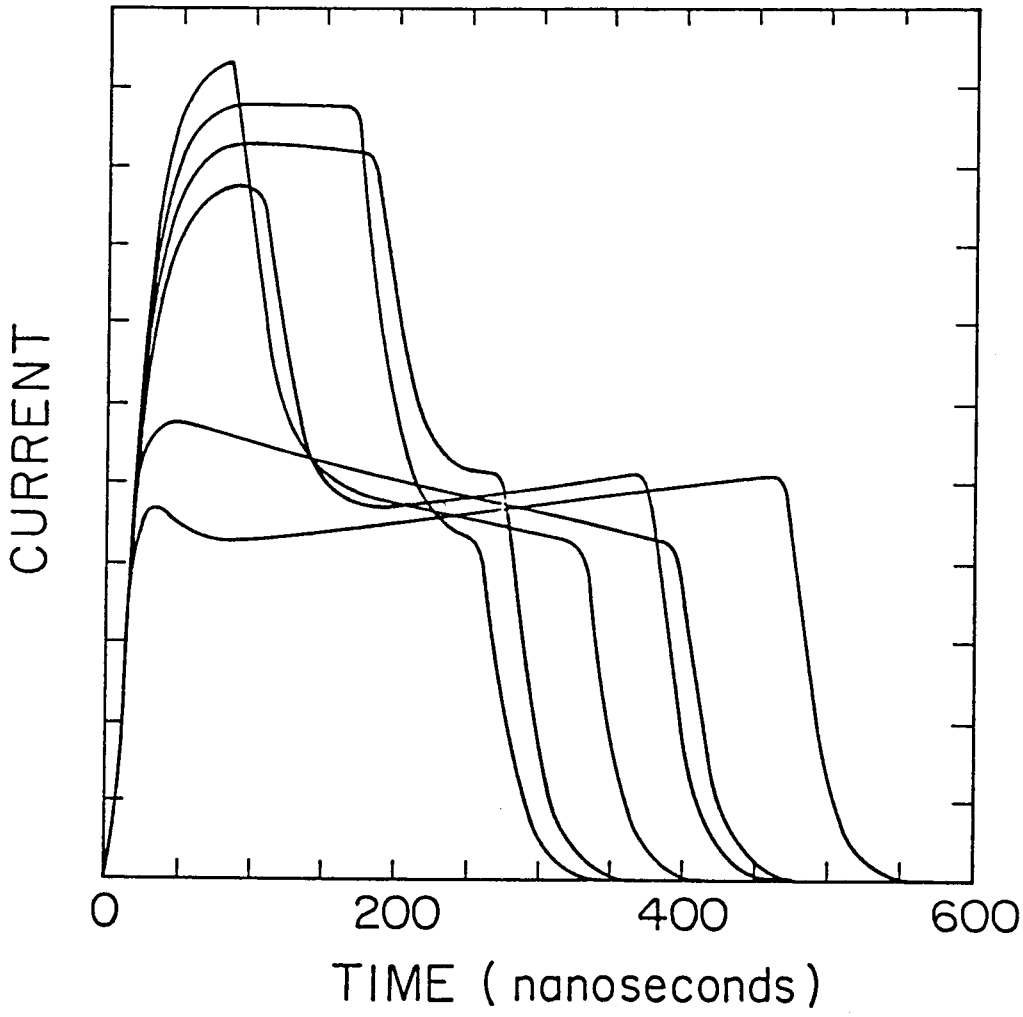

Figure 13. Computer simulation of the current pulse waveform in a 3 cm thick planar detector for energy depositions at locations 0.5 cm apart.

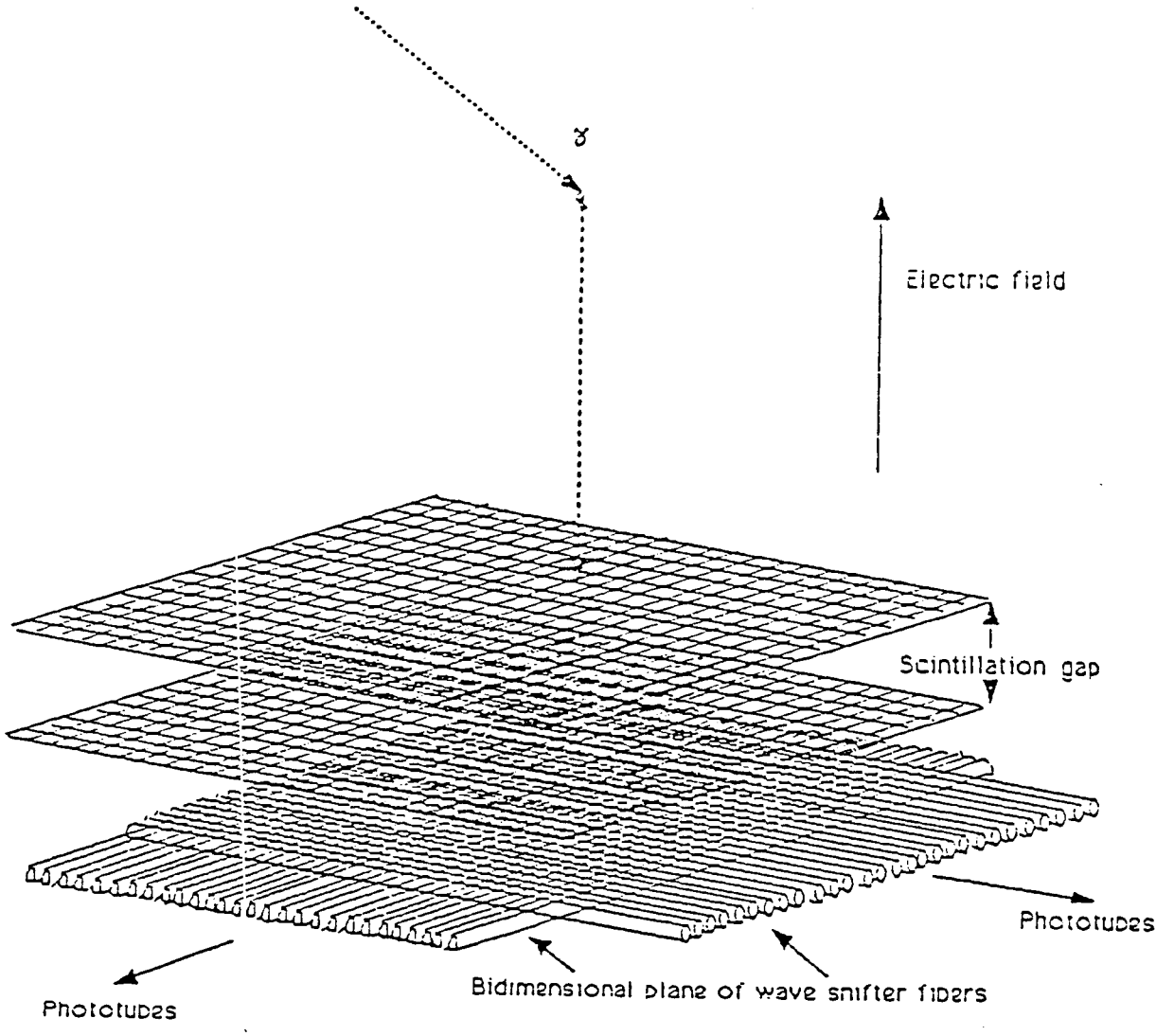

Figure 14. Schematic of gas scintillation drift chamber with wave shifter fiber readout.

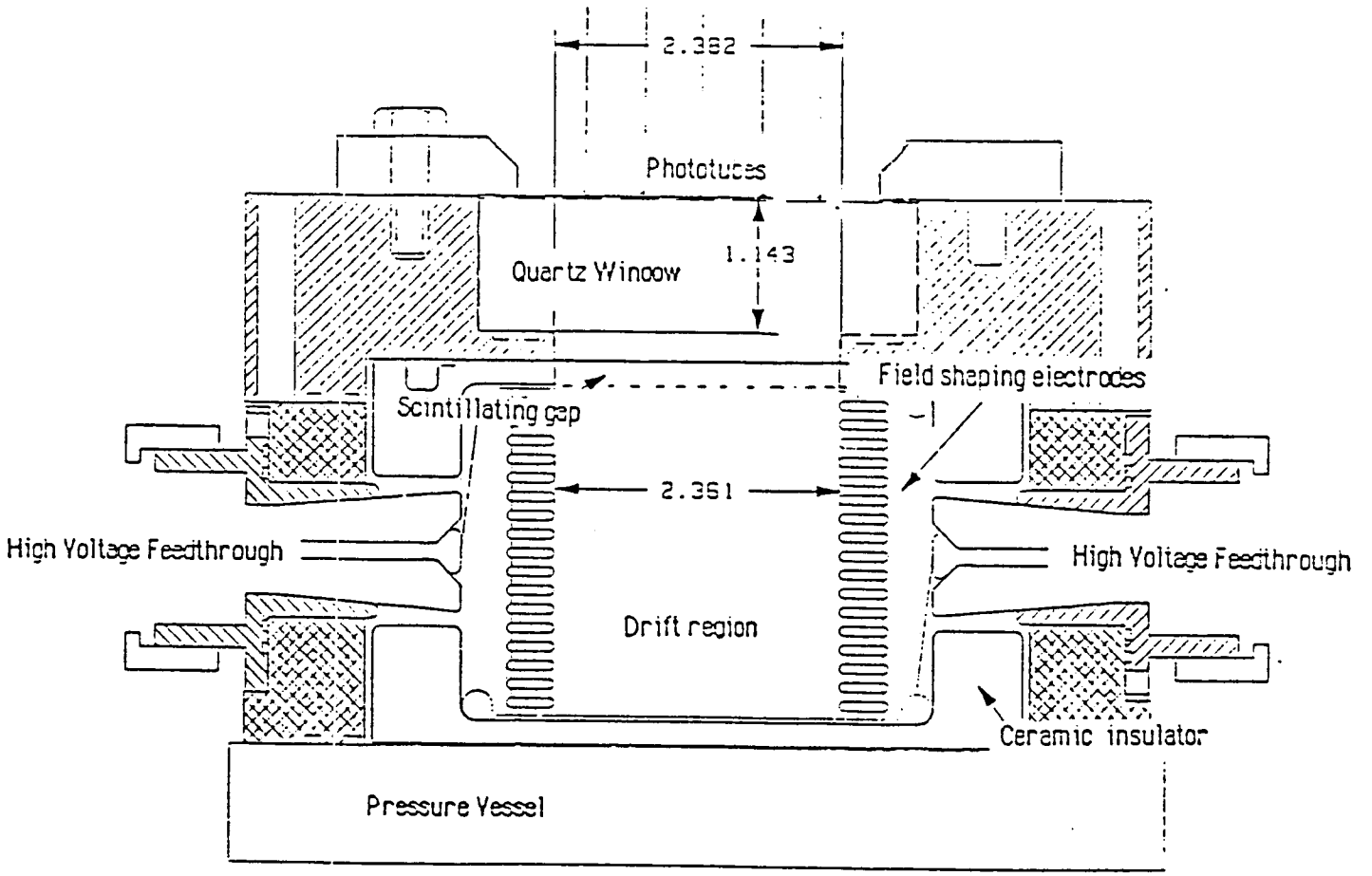

Figure 15. Engineering drawing of prototype being built (Auger camera configuration).

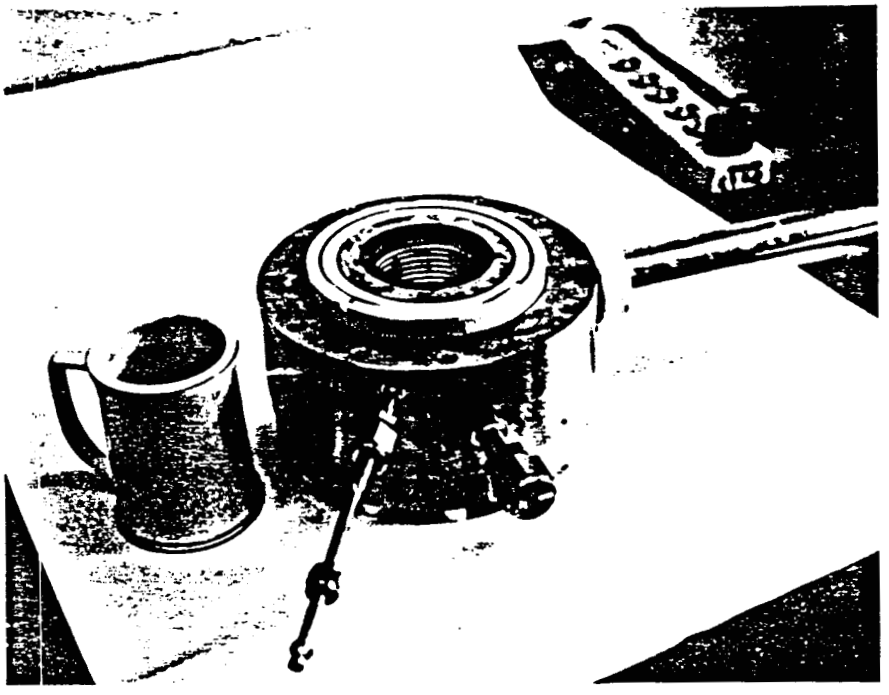

(a)

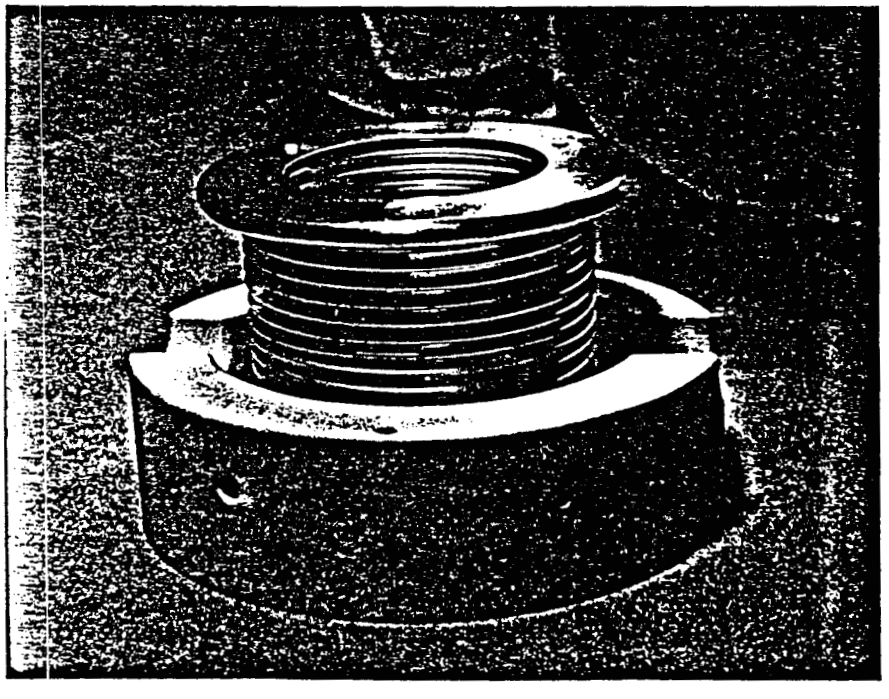

(b)

Figure 16. (a) Outer housing with field shaping electrodes and ceramic insulator. (b) Field shaping electrodes and ceramic insulator.

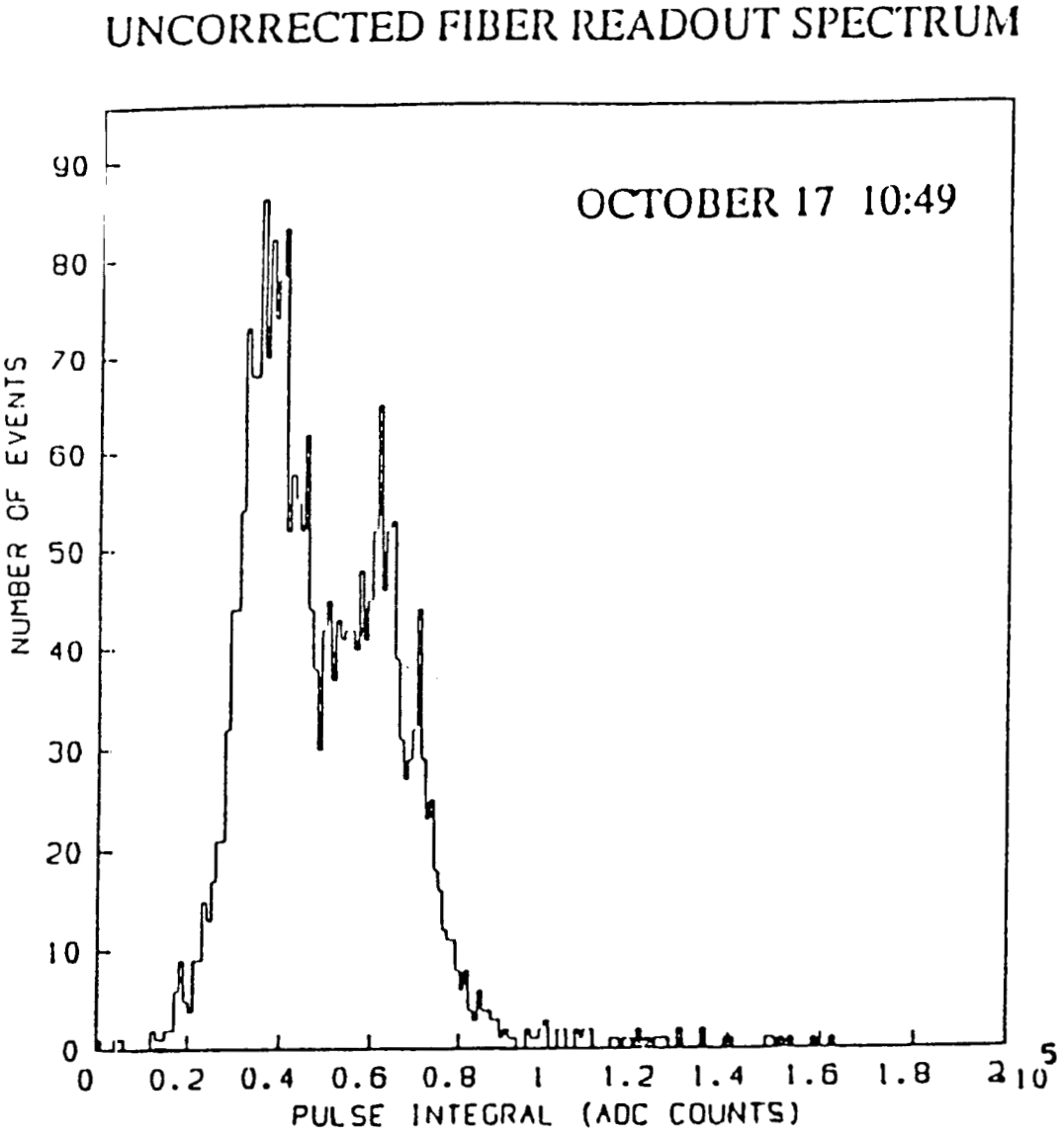

Figure 17. ^{241}Am uncorrected spectrum observed in our gas scintillation drift chamber with wave shifter read-out.

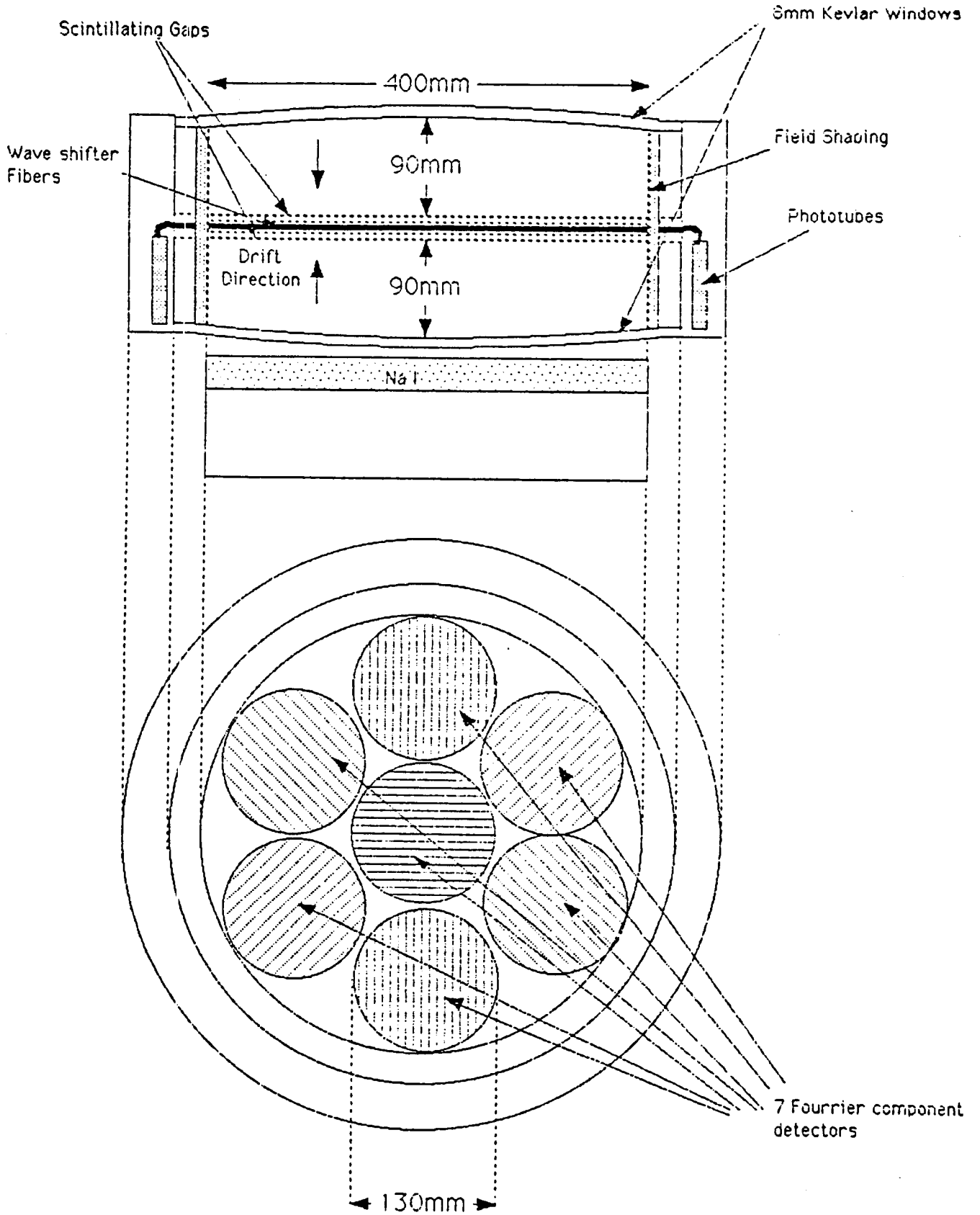

Figure 18. Schematic of high pressure (10 atmosphere) xenon gas scintillation drift chamber for solar hard X-ray imaging.

Appendix A
HIREGS Instrumental Details

Background Rejection by Pulse Waveform Analysis

In modern germanium gamma-ray detector systems the background consists of: a) diffuse sky cosmic (and atmospheric) hard X-ray and gamma-ray fluxes in the open aperture of the detector system; b) leakage of ambient γ-rays through the shield, and c) internal background in the detector, now known to be almost entirely due to radioactivity induced by cosmic rays and trapped protons and their secondary neutrons. *Gehrels* (1985) has analyzed the internal radioactivity background in germanium detectors and found that the part not anticoincidenced by the active shield consists primarily of β^--decays.

The energy deposition range of a β^--particle is small, e.g., 0.08 cm at 1 MeV, and it can be said to deposit its energy at a single site. On the other hand, at energies above ~200 keV, because of Compton scattering (and pair production at >2 MeV), photons typically have multiple site energy loss signatures. Thus, by distinguishing between single and multiple site interactions in the detector volume, it is possible to reject most of the induced radioactivity background at energies from a few hundred keV to several MeV.

Techniques have been developed at UCB to efficiently separate single-site from multiple-site interactions. Gamma-rays which lose part of their energy in the front segment and the rest in the rear segment would be identified by front-rear coincidence. For purely rear segment events, pulse shape analysis is used in HIREGS to identify multiple-site interactions located at different radial distances.

The energy deposited in the Ge detector at a given site produces charge carriers, electrons and holes, which travel radially in the electric field of the detector to the central and outer contacts. The motion of the charge carriers induces a current at the electrodes; the integral of the current signal is proportional to the total charge. The current pulse waveform at the preamplifier input depends on the radial location of the site of energy deposition. When the energy deposition of a multiple-site interaction is distributed in radius, the pulse waveform becomes a superposition of single-site pulses.

Figure B1 shows examples of single-site and multiple-site current pulses observed from a segmented coaxial Ge detector flown in February 1988. At UCB we have calculated the detailed shape of the current pulse waveform for single-site energy losses typical of single photopeak absorption events and β^--decay radioactivity, and for normal photons, using the distributions of energy depositions resulting from the Monte Carlo photon propagation program (*Roth, Primbsch and Lin,* 1984, attached to this Appendix). Our calculations indicate that for a uniform Ge detector with near ideal noise characteristics it may be theoretically possible to reject $\gtrsim$95% of the single-site events while retaining $\gtrsim$80% of the multiple-site events at ~800 keV energy. With current available balloon flight pulse waveform analysis electronics we have achieved ~90% singles rejection with ~70% retention of multiple events at ~800 keV in the laboratory (*Smith et al.*, 1988, attached to this Appendix). Figure 12 (main proposal) shows that the HIREGS background in the 0.4–2 MeV gamma-ray line region would be reduced by a factor of ~2–4. Since the sensitivity is proportional to signal/$\sqrt{\text{background}}$, this would give a gain of a factor up to 1.4 in sensitivity. To place this in perspective, up to twice as many Ge detectors would be required to achieve the same sensitivity without segmentation and pulse shaping techniques.

A single dual segment Ge detector with this pulse waveform analysis electronics was flown by our group in February 1988 on a long duration balloon flight. The detector was enclosed in a CsI annulus and bottom shield and had a NaI front collimator which defined a 15° FWHM field of view. The pulse waveform analysis data from that flight provided the first measurements of the β^--decay background at balloon float altitudes. The β^--decay background for HIREGS plotted in Figure 12 (main proposal) is based on these measurements. A Monte Carlo program was used to model the shield and Ge detector for the instrument flown in February 1988. The actual observed flight shield leakage background spectrum was used to normalize the Monte Carlo, and the same normalization factor applied to a Monte Carlo simulation of the HIREGS shield to provide the shield leakage background plotted in Figure 12 (main proposal).

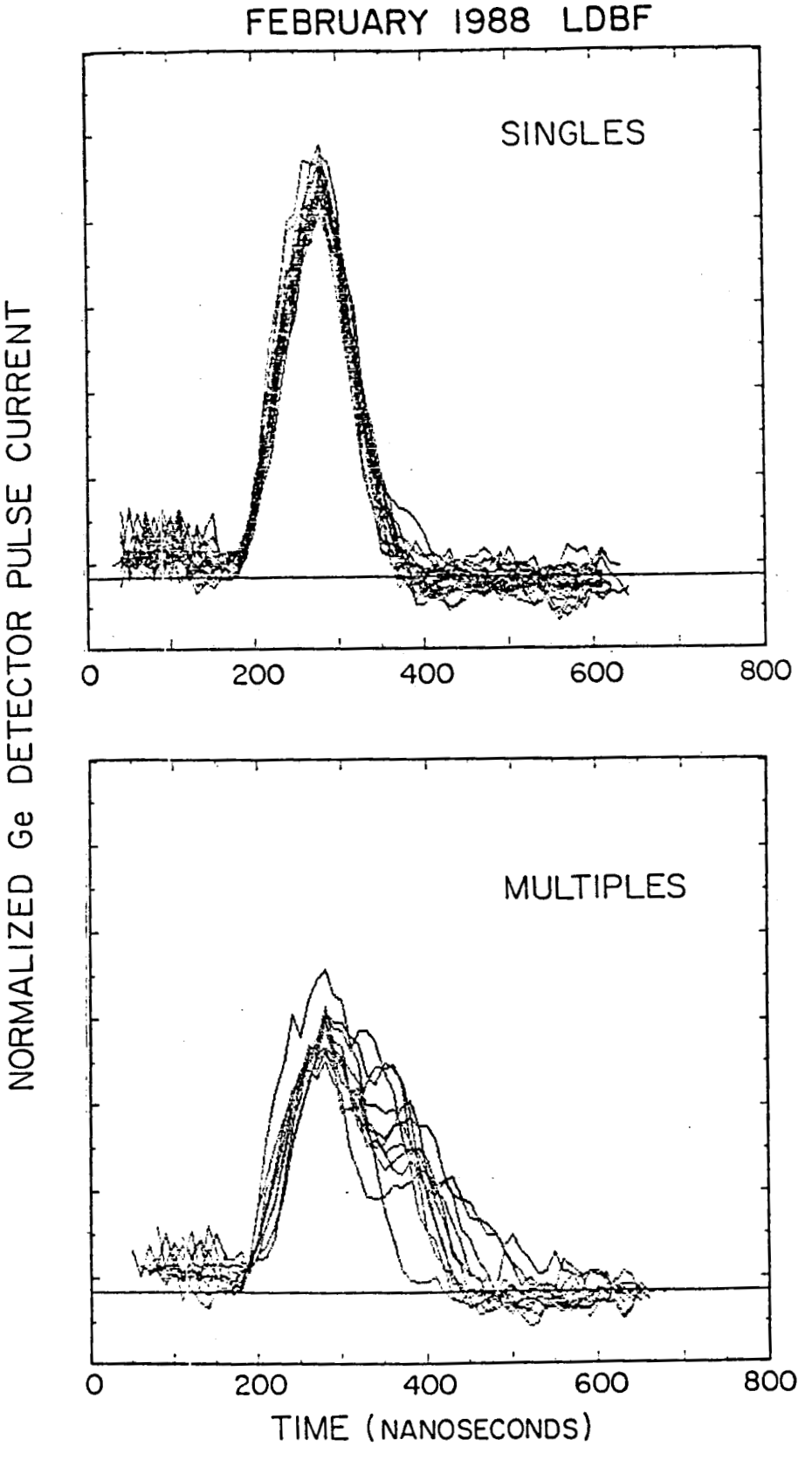

Figure B1. Current pulse waveforms observed on the February 1988 balloon flight from the rear segment of a two segment Ge detector similar to those proposed for HIREGS. The upper panel shows single-site energy depositions, presumably β^--decays while the bottom panel shows multiple-site interactions.

For HIREGS, as in our February 1988 flight instrument, the pulse waveform data will be brought to the ground for the type of analysis described in *Smith et al.* (1988). We are presently developing algorithms for on-board pulse waveform analysis.

Dynamic Range

The division of the Ge detector into two electrically independent segments is crucial for high spectral resolution measurements of solar flare gamma-ray lines in the presence of intense hard X-ray fluxes. Long shaping times, pulse pile-up rejection, and baseline restoration are required to obtain high spectral resolution. These requirements imply that for a pulse to be accurately analyzed no new pulses can occur within a fixed interval (typically tens of μs) of the original pulse. Using Poisson statistics for an interval distribution, we have computed the rate of analyzed events to incoming photons (Figure B2). For the very largest gamma-ray line flares the incoming photon rate in $\lesssim$0.2 MeV range for a unsegmented Ge detector can be $\gtrsim 10^5$ c/sec. At that rate only ~4% (4×10^3 events/sec) of the incoming photons would be analyzed for a 32 μs dead interval typical of normal high resolution Ge electronics. For the exceptionally fast system proposed here, with 4 μs shaping and ~13 μs dead interval, ~27% (~2.7×10^4 counts/sec) of the incoming photons would be analyzed. This is not a serious problem for the low energy $\lesssim 10^2$ keV hard X-rays which dominate the rate (the true rates are provided by the fast amp with 400 ns shaping time), but is a disastrous drop in efficiency for gamma-ray line observations in the same detector.

In a HIREGS Ge detector the front and rear segment have completely separate electronics. The rear segment event rate (for any interaction) is less than $\sim 4 \times 10^3$ c/s for the largest reported flare of the last solar cycle. At that rate ~95% of the rear segment events are cleanly analyzed with high spectral resolution, thus maintaining the large effective area even in large flares. We have conducted laboratory tests with input rates of up to 2×10^5 c/s in the front segment simultaneous with gamma-ray line rates of up to 5×10^3 c/s in the rear segment and verified that there is no significant dead time, nor any measurable degradation in resolution, for the rear segment.

Note that in the Ge detectors presently being developed with the outer contact divided into multiple segments (*Varnell and Pehl*, 1988), the signal from the inner contact is used for all the high resolution energy measurements while the outside segment signals are only used for identifying the segment. Since the inner contact collects pulses from the entire detector, this type of multiple-segment detector will have the same throughput rate as an unsegmented detector; that is, in a large flare only a small fraction of the events will be analyzed.

Bismuth Germanate Shield

The anticoincidence shield plays a particularly important role in a sensitive spectrometer such as the one proposed here. It must not only reduce the continuum background, which is of atmospheric and cosmic origin, but also, it must be extremely efficient in rejecting the 511 keV line produced in the atmosphere. Calculations demonstrate that if the shield is not 99% efficient at 511 keV, the line background at this energy will seriously compromise the performance of the spectrometer. Thus we have taken 1% transmission at 511 keV as a shield performance specification. A comparison of commonly used scintillators (CsI, NaI, and BGO) clearly demonstrates that BGO is not only the most cost-effective anticoincidence material (i.e., it minimizes the number of dollars per 511 photon absorbed), but also the most mass- and volume-effective (i.e., it minimizes the number of grams and cc's per photon absorbed). For this reason, and also because the laboratories involved in this collaboration have built a BGO shield for a similar spectrometer for cosmic sources (the UCSD/UCB/CESR/Saclay balloon gamma-ray spectrometer), we have chosen a BGO shield for the proposed instrument. The geometry is a 5 cm thick well surrounding the cryostat, with a 5 cm thick blocking plate below it (Figure 2, main proposal). Since BGO is not yet readily available in diameters much larger than three inches, the shield will be built up out of 48 BGO section in 9 housings. This architecture was also used for the cosmic balloon spectrometer, and poses no particular problems. The nominal design calls for one photomultiplier to be associated with each BGO piece (48 PMT's in all). The PMT currently being used is the Hamamatsu 1847, and the electronic design used places a high voltage power supply and preamplifier at the base of the tube. A lower energy threshold of ~50 keV is achieved with this configuration. In the interest of reduced mass, volume, and complexity, we are studying an alternate possibility, namely attaching one or

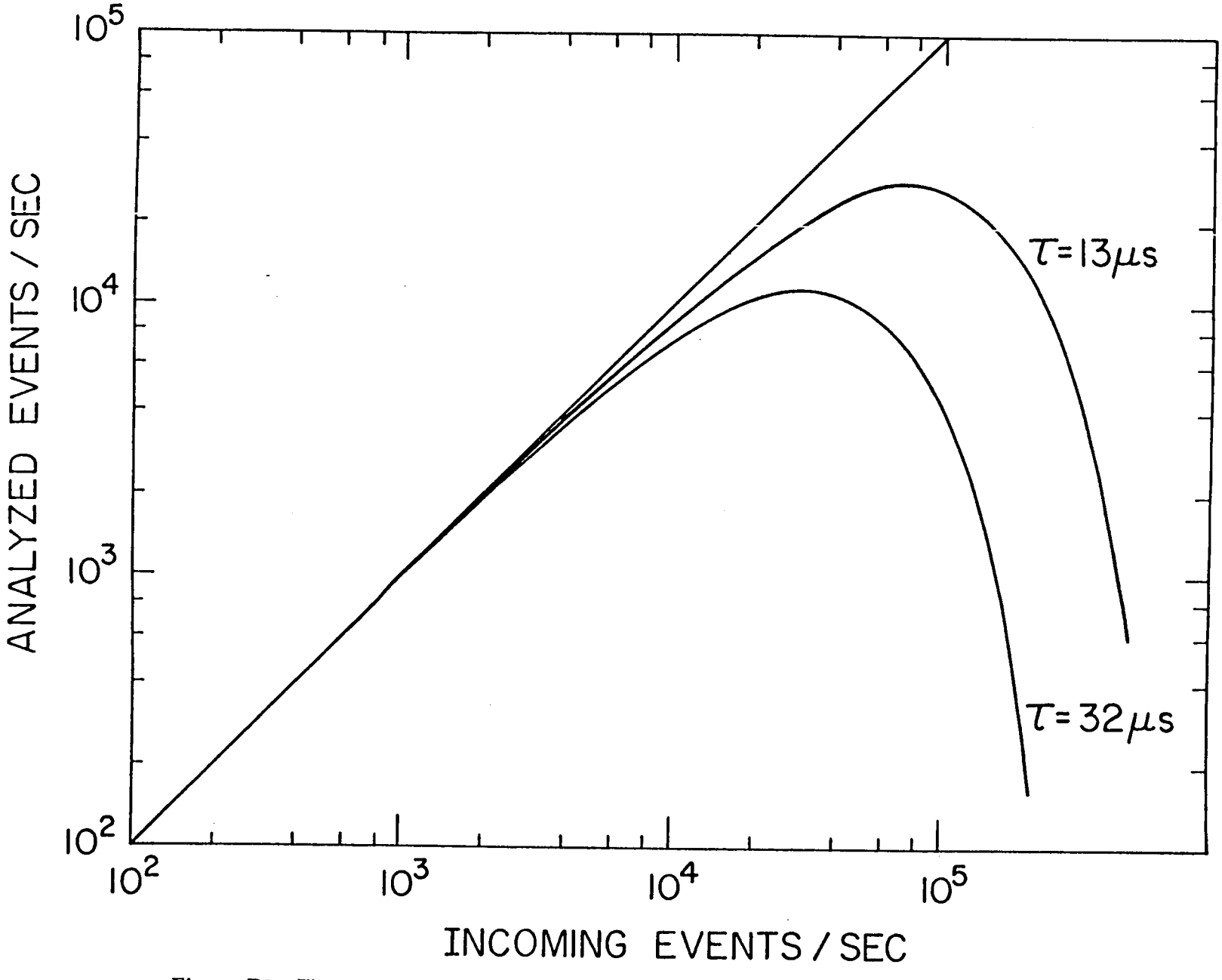

Figure B2. The rate of analyzed events is plotted here versus the incoming event rate for two different dead times.

more photodiodes to each BGO bar. Large area photodiodes (1 × 2 cm) are now available (e.g., the Hamamatsu 2744) with sensitivity curves optimized for BGO. In addition to the mass reduction associated with replacing PMTs by photodiodes, there would be a substantial volume reduction, and low voltage (25 volt) supplies would replace the high voltage needed for PMTs. Tests are presently underway at UCB to determine whether this is a viable alternative.

We currently envisage the shield construction as a task which will be shared between the CESR and UCB. CESR would use its current electronic design for the PMT preamps and high voltage supplies, and its current mechanical design for the BGO and PMT housings. In addition, the CESR would supply the BGO annulus, and UCB would purchase the BGO rear shield. The shield GSE would be built at CESR. Assembly and pre-deliver checkout (a labor-intensive task) would take place in France.

Hard X-ray Measurements

Almost all of the measurements of solar flare hard X-ray and gamma-ray burst continuum spectra have been made with scintillation detectors. The poor energy resolution of these detectors inherently limits the steepness of the continuum spectra that can be measured. Furthermore, the observed spectra must be deconvolved by assuming an *a priori* spectral shape, convolving it with the detector response, and comparing the result with the actual observed count rate spectrum. As pointed out by *Fenimore et al.* (1982), this procedure can lead to artifacts in the spectra. In addition, small changes in gain and/or dead layers will strongly affect the results. Finally, nonlinearities and K-edge effects in the middle of the hard X-ray range further complicate the interpretation of the spectra.

The very high resolution of germanium detectors eliminates the need for any *a priori* assumptions of a spectral shape and allows a simple direct deconvolution of the count rate spectrum to obtain the incident photon spectrum (see *Lin and Schwartz*, 1987, in Appendix A). Germanium detectors are inherently linear and the germanium K-edge is well below the 20 keV threshold. The gain stability of our previous 4 detector germanium system was such that the data from all four detectors could be summed over the duration of the entire 1980 flight with less than 1 ch (~0.14 keV) line broadening. The reverse bias germanium detectors used in HIREGS have an extremely thin ion-implanted outer surface, essentially transparent to >20 keV hard X-rays and gamma-rays.

Analog Electronics

Each Ge detector has independent signal paths for the front and rear segments as indicated in Figure B3. The analog electronics is essentially the same as used in the UCB/UCSD/CESR cosmic gamma-ray balloon system. For each signal path (*Landis et al.*, 1970), this includes a cooled FET, wide bandwidth charge sensitive preamplifier, followed by dual shaping amplifiers. A slow shaper-amplifier (~4 μs time constant) is used for pulse height analysis, and a fast shaper-amplifier-discriminator (~400 ns) supplies fast pulses for coincidence, pileup rejection, timing, and rate accumulations. (The two amps are not shown separately in Figure B3.) The pile-up rejection system, together with a gated baseline restorer, allows operation at incoming photon rates up to $\gtrsim 3 \times 10^5$ s^{-1} per detector without resolution degradation.

The shaped pulses go to a Pulse Height Analyzer (PHA). For energies below 2.5 MeV, the 12-bit PHA analyzes events directly with ~0.6 keV per channel resolution. For energies in the range of 2.5 to 16.3 MeV, a gain change discriminator causes the shaper-amplifier gain to be reduced by a factor of 6.5 before passing the event to the 12-bit PHA, resulting in ~4 keV per channel resolution. The gain status is latched in the PHA as a 13th bit. Three additional coincidence status bits (front-rear coinc, det-det coinc, and det-shield coinc) are provided to each PHA to be latched at the time of the event trigger.

For energies above 16.3 MeV, an Upper Level (UL) discriminator inhibits the 12-bit PHA and triggers a separate 6-bit flash PHA. This PHA covers the energy range of 16.3 MeV to approximately 250 MeV. The CsI collimator and BGO rear shield also have 6-bit flash PHAs to cover the $\gtrsim$0.3 MeV to $\gtrsim$250 MeV energy range.

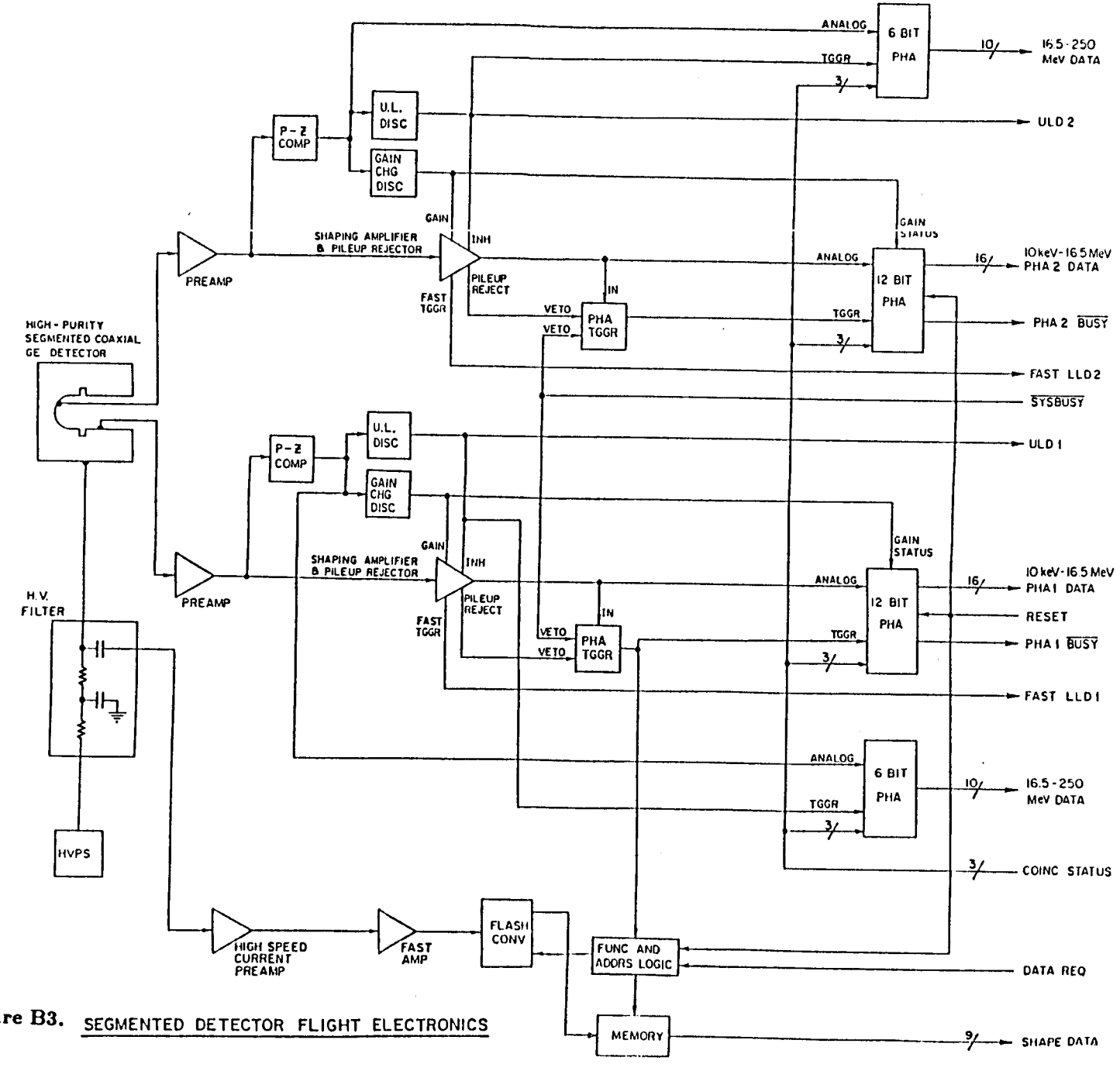

Figure B3. SEGMENTED DETECTOR FLIGHT ELECTRONICS

Current Pulse Waveform Electronics

A third signal path from each detector consists of a high-speed current preamp, a fast amplifier, a flash converter, a fast memory, and the necessary support logic (Figure B3). The current preamplifier is connected to the outer surface of the detector through the high voltage filter network. Its output signal is the current waveform that results from the charge collection process in the detector, which typically takes ~200–300 ns. A fast amplifier provides gain and buffering of the signal to drive the input of a 9-bit flash converter operating at 100 Msamples/sec thus providing 10 ns samples of the waveform. The digitized samples are stored in a high speed memory operating as a circular buffer. This process operates continuously until an event trigger to the rear segment PHA stops the storage process. Since the event trigger occurs 4 μs after the event (due to the shaper-amplifier peaking time of 4 μs) the circular buffer must be sized to approximately 4.1 μs in length (i.e., 410 samples) to provide some pre-event background. At the arrival of the stop pulse, the memory address logic then points to the locations in memory where an event of 4.1 μs earlier is stored. Consequently, the 64 ten-nanosecond waveform samples can be read out of the memory merely by incrementing the address with each data request. A final reset pulse to the PHAs and the waveform logic restarts the 100 Mhz digitization and storage into the circular buffer. The current pulse waveform data for 0.4–2 MeV events are stored by the data system and analyzed on the ground.

Data System

Because the experiment is designed to see bursts of information arriving at potentially very high rates, each channel uses a dedicated microprocessor to guarantee no loss of data. As shown in Figure B4, the pulse heights for each segment and the rear segment waveform shape data would be analyzed by its own microprocessor which would add timing to ~1 ms, detector identification and coincidence information for a photon event total of 4 bytes (32 bits) and a waveform event total of 76 bytes. There is a separate interface to count the events detected by the collimator and shield, as well as to provide master clock timing information to each of these processors.

In the 0.4–2 MeV energy range, for rates up to several times quiet background, waveform events from the rear segment are sent to the main processor which stores them on VCR tape. From background up to flares with total rates of $\sim 5 \times 10^4$ analyzed events/sec, every photon event is stored. For larger flares (which occur on average only about once every ten days) all analyzed photon events with energy above 0.4 MeV (i.e., in the gamma-ray line region) are stored. All low energy (<0.4 MeV) photon events are accumulated into 256 ch pulse height spectra which are then stored; the time resolution for these spectra increases with event rates. In addition, a fraction of the low energy photon events are stored, up to a maximum VCR storage input rate of 256 kbytes/s. The true counting rates for all Ge detectors obtained from the fast amplifiers (0.4 μsec shaping time), as well as shield count rates and dead times, are stored as well.

The main processor collects the data from each of the channel processors and is responsible for storage to the VCR tape system as well as for telemetry to the ground when desirable. This computer, with its large buffer memory to provide temporary data storage, is very similar to what has already been flown. As in our previous long duration balloon flights (LDBF), two telemetry modes are planned: (1) directly to ground station via line-of-sight telemetry, and (2) via the INMARSAT geosynchronous satellites when outside of line-of-sight to ground station. Our group has already developed a balloon-borne two-way link using a pointed 1 meter dish capable of ~1200 baud transmission through INMARSAT. The main microprocessor would select, format, and store the data for INMARSAT transmission.

The VCR tape storage units are also similar to what has been used in previous flights, but here two units are needed to provide redundancy and the necessary storage capacity for up to 30-day flights.

The other functions the main processor performs such as command, navigation, pointing and housekeeping are also similar to those of our recent LDBF flights and those developments could be directly applied to this experiment.

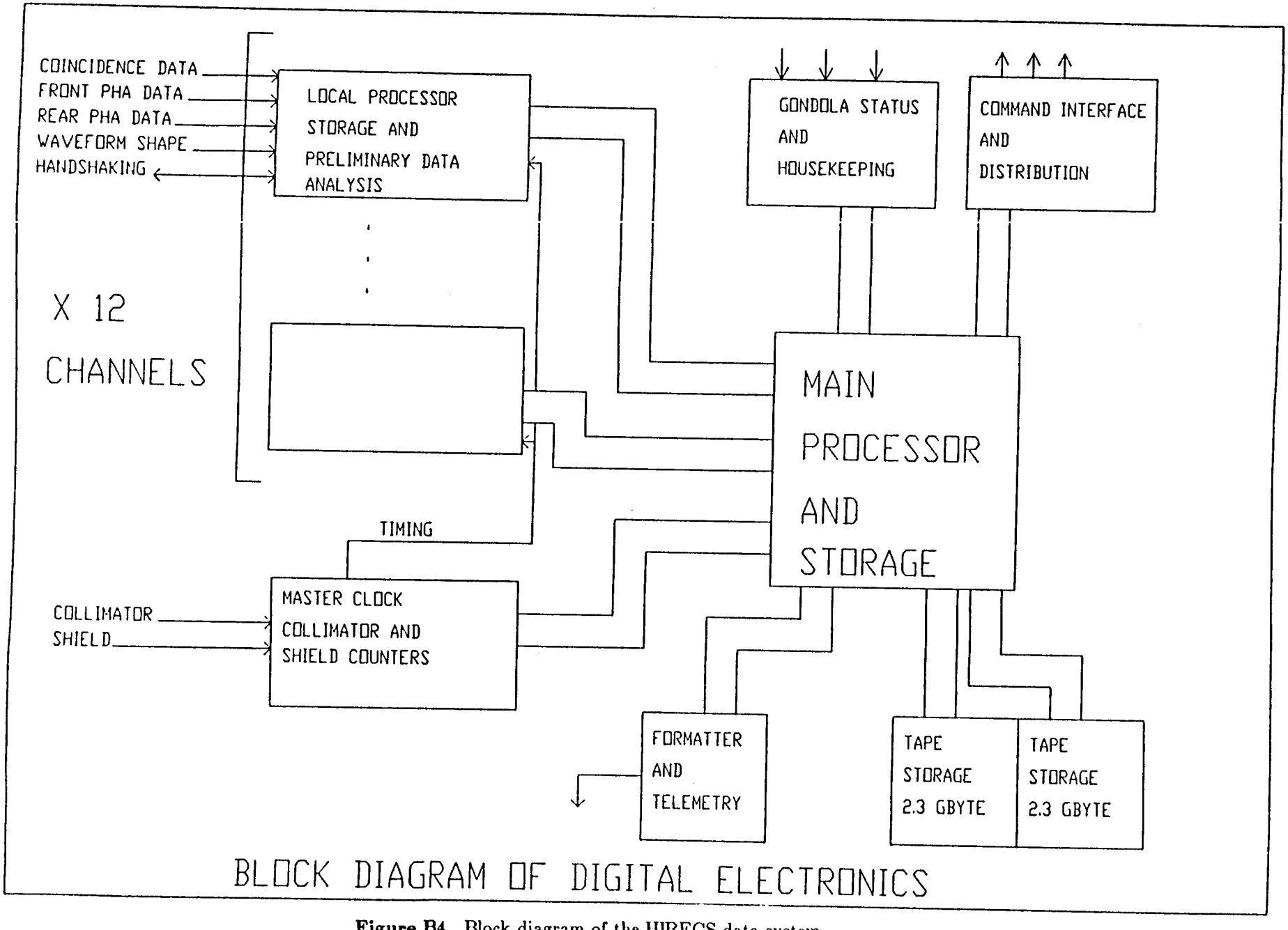

Figure B4. Block diagram of the HIREGS data system.

A LONG-DURATION BALLOON PAYLOAD FOR HARD X-RAY AND GAMMA-RAY OBSERVATIONS OF THE SUN

R.P. LIN, D.W. CURTIS, J.H. PRIMBSCH, P.R. HARVEY, W.K. LEVEDAHL,[1] D.M. SMITH[1]
Space Sciences Laboratory, University of California, Berkeley, CA 94720

R.M. PELLING, F. DUTTWEILER
CASS, University of California, San Diego.

K. HURLEY[2]
CESR, Toulouse

ABSTRACT. We describe a balloon payload designed to study the processes of energy release, particle acceleration, and heating of the active corona, in hard X-ray microflares and normal flares. An array of liquid nitrogen-cooled germanium detectors together with large area phoswich scintillation detectors provide the highest sensitivity (~500 cm^2) and energy resolution ($\leq$0.7 keV) ever achieved for solar hard X-ray (~15–600 keV) measurements. These detectors were flown in February 1987 from Australia on a long duration RAdiation COntrolled balloON (RACOON) flight (LDBF) which provided 12 days of observations before cutdown in Brazil. The payload includes solar cells for power, pointing and navigation sensors, a microprocessor controlled data system with VCR tape storage, and transmitters for GOES and ARGOS spacecraft. This successful flight illustrates the potential of LDBF's for solar flare studies.

1. INTRODUCTION

Because of the Challenger disaster and the current bottleneck in the Explorer program, it appears highly unlikely that any NASA spacecraft for solar flare studies can be launched for the next solar maximum. The ESA/NASA Ulysses (formerly Solar Polar) mission, to be launched in 1990, will have a solar flare X-ray instrument aboard (Cotin *et al.*, 1983). Present plans call for a small Japanese spacecraft, Solar A, dedicated to solar flare studies, with U.S. participation in a soft X-ray telescope as part of the payload, to be launched in 1991. Some solar flare measurements will also be made by the Gamma-Ray Observatory (GRO). Crucial new spectroscopy and arcsecond imaging observations in the gamma-ray and hard X-ray range will not, however, be done by these missions. Long duration balloon flights (LDBF) offer an attractive way to obtain these measurements during the next solar maximum. Because energetic photons and neutrons are able to penetrate the upper layers of the earth's atmosphere, high altitude balloons can provide a means for obtaining excellent quality observations of these flare emissions. Furthermore, the long observing periods required to catch large gamma-ray

[1] Also Physics Department
[2] Presently at Space Sciences Laboratory, University of California, Berkeley CA 94720.

Solar Physics 113 (1987) 333–345.

or neutron flares are now within reach of LDBF's. In addition, high-resolution optical measurements, free of the seeing effects and cloud cover of ground-based observations, can be made by balloon-borne instruments.

Large, powerful instruments, up to ~3000 lbs. total payload weight, can be carried by the present standard 28.4 million cu. ft. balloons to altitudes of ~130,000 ft. (40 km). At that altitude there is less than 3 g/cm^2 of overlying atmosphere, so high quality hard X-ray and gamma-ray measurements down to ~15 keV are possible. For standard zero-pressure balloons the temperature of the gas, and therefore the balloon altitude, is controlled by the radiation received from the Sun and the Earth. Thus the balloon is at high altitude during sunlight hours but drops during nighttime. If the balloon initially reaches a high daytime float altitude it will remain above the tropopause in its day-night excursions under normal conditions without ballast drops. Then, in this simple RAdiation COntrolled balloON (RACOON) mode (Lally, 1982), flight durations are limited only by balloon lifetime and gas losses (which can be offset by ballast drops).

LDBF's in the RACOON mode can provide 12–20 days at float altitude by circumnavigating the globe. During the three-month summer season at mid-latitudes, strong stable zonal winds flow with high velocity approximately along latitudinal lines, so circumglobal flights are feasible. At present, around-the-world flights are possible only in the southern hemisphere, for political reasons. Trans-pacific flights from the U.S. to China, however, can offer 5–10 day durations in the northern hemisphere summer. LDBF's are also possible year-round at equatorial latitudes, provided adequate launch and recovery sites can be found.

The main characteristics of RACOON LDBF's are:

- The balloon is at high altitude during sunlight hours but drops during nighttime, making RACOON flights particularly suitable for solar observations. LDBF's from south pole could provide 24 hour/day coverage of the sun, although at large sun-zenith angles.
- Essentially $\gtrsim$12 hours of continuous high altitude observations are obtained each day, as compared with typical low-altitude earth-orbiting spacecraft (such as SMM), which have an ~95-minute orbit with ~40 minutes earth shadow each orbit. For SMM, the start or decay phase of a large flare can be missed. Coverage through an entire flare including at least 1000 s after the impulsive phase is important to obtain the delayed emissions from positron annihilation, neutrons, etc., and to observe the effects of delayed acceleration in large flares.
- The background for hard X-ray and gamma-ray measurements at balloon altitudes is particularly low and very stable, unlike the background for low altitude spacecraft, which changes drastically through the orbit. Thus, the effective sensitivity is significantly greater and data analysis is far simpler. Since the energetic particle radiation environment is much less severe at balloon altitudes than for low orbiting spacecraft, activation of the detector and radiation damage to the electronics are negligible.
- It is simple and cheap to provide cryogenic cooling for balloon-borne instrumentation but expensive and complex solid-cryogen or mechanical coolers are required for spacecraft because of the weightless environment in orbit.
- Because of the much more benign launch environment and the capability for repairs after each flight, balloon experiments need not be designed to space-qualified specifications. These are major cost drivers for space experiments.

In 1983 a 15 million cubic ft. balloon with an ~1200 lb payload (from Case Western Reserve University, see Koga *et al.*, 1985), designed to search for solar flare

Appendix B

neutrons, was launched from Alice Springs, Australia, and made a circumnavigation of the globe in the southern hemisphere in ~18 days. The ground command cutdown of the payload from the balloon malfunctioned, however, and the balloon continued past Australia. After 22 days the automatic cutdown was triggered and the payload was parachuted into the Indian Ocean.

In 1987, two exploratory RACOON balloon flights were launched from Alice Springs, Australia. One of them (from Louisiana State University) was a passive stack of emulsions for cosmic ray studies. The other payload, described in detail here, carried a complement of hard X-ray and gamma-ray detectors, including both liquid-nitrogen cooled germanium detectors for high spectral resolution and large-area phoswich scintillation detectors for high sensitivity, for observations of microflares and flares from the sun. Both these payloads were carried by the standard, 28.4 million cubic ft., 0.8 mil polyethylene, zero-pressure balloons developed for normal short-duration flights. The solar payload was designed for automated continuous 24 hours/day operation with $\gtrsim$8 hours/day of solar observations and ~6 hours/day of non-solar observations at nominal daytime altitude float, and 10 hours/day at lower nighttime altitudes. Below we describe the detectors, the balloon gondola and ballast system, the power system, the pointing and navigation system, data and telemetry systems, etc. Table I summarizes the payload capabilities. Figure 1 shows a schematic of the payload.

This payload was developed and fabricated by the Space Sciences Laboratory, University of California, Berkeley, in collaboration with the Lawrence Berkeley Laboratory, the University of California, San Diego, and the Centre d'Etude Spatiale des Rayonnements, Toulouse, France.

2. DETECTORS

A 50 cm^2 array of four 1.3 cm thick planar germanium detectors cooled by liquid nitrogen and surrounded by a CsI/NaI anticoincidence well provides high spectral resolution ($\lesssim$0.7 keV FWHM) measurements of hard X-rays and gamma-rays from ~13 to 600 keV (Lin *et al.*, 1981). A 160 liter dewar provides a cooling lifetime of $\gtrsim$20 days. The detectors point straight up with a field of view of ~30° FWHM.

Two 3 mm NaI/38 mm CsI phoswich scintillators, one 300 cm^2 and one ~200 cm^2 (Matteson *et al.*, 1977), provide for high sensitivity measurements of hard X-rays between ~20 and 300 keV. These detectors are collimated to ~15° FWHM field of view and pointed by an alt-azimuth pointing system to ~1° accuracy. On-board pulse shape discrimination circuitry is used to provide very low background 20-30 keV and 30-50 keV rate channels.

Every photon detected by these two detector systems is analyzed for pulse height (4096 channels for the germanium detectors and 64 channels for the scintillators) and for pulse shape in the case of the phoswich. A combination of burst triggers identifies and preferentially stores impulsive burst data for readout at ~60 bps via geosynchronous spacecraft (GOES) to ground stations. All the data for every detected photon are stored by the on-board VCR tape system for eventual transmission to the ground by VHF link when the balloon returns to the launch site, and also are available upon cutdown and recovery of the payload.

A set of new solar total irradiance detectors is also on-board for testing.

TABLE I: Long duration balloon flight capabilities

Flight Characteristics		
	Duration:	15-20 days
	Path:	Circumglobal flight at ~-23° latitude, launch and recovery at Alice Springs, Australia
	Altitude:	130,000 ft daytime, 110,000 night
	Tracking:	to $\lesssim$100 km by ARGOS satellites
Balloon		
		28.4 million cu ft, zero pressure polyethelene
Gondola		
	Size:	9 ft×5 ft×7 ft high
	Weight:	2100 lbs + 900 lbs ballast
Power System		
		Solar cells and lead-acid batteries providing 90 watts continuous (24 hr/day)
Pointing and Navigation System		
	Aspect system:	Simple sun tracker and magnetometers to provide $\lesssim$1° accuracy
	Navigation system:	Balloon location (latitude longitude) determined on board once/day to ~1°.
	Pointing:	Alt-azimuth system with $\lesssim$1° accuracy for for sun pointing and offset pointing
Data and Telemetry System		
	Total data volume on tape:	6-18 Gigabits = 370–2200 million 16-bit events (depending on selected record speed of VCR). This includes nominal data block gap overhead.
	Maximum data rate:	40,000 (16-bit) events/s continuous 400,000 events/s burst
	Tape buffer memory size:	750,000 events (easily expandable to 3,000,000 events)
	Event timing accuracy:	1 millisecond time tag every 14 events
	GOES/METEOSAT/ HIMAWARI data rate:	60 bits/s
	VHF real-time data rate:	8 Kbits/s
	VHF tape play-back rate:	256 Kbits/s

3. GONDOLA

The outer frame of the gondola is a structure approximately 9 ft. long by 5 ft. wide by 7 ft. high (Figure 1). Within this frame is a styrofoam box of 4-inch wall thickness coated with aluminized mylar on all surfaces. Thermally insulating spacers extend through the styrofoam to support the inner frame structure which holds all of the components.

The collimated and pointed scintillator detector assembly is mounted at one end of the inner frame at a location such that the field of view is clear for all pointing directions. The germanium detector assembly is mounted at the other end of the frame for a clear vertical field of view. As this instrument utilizes high-purity germanium detectors,

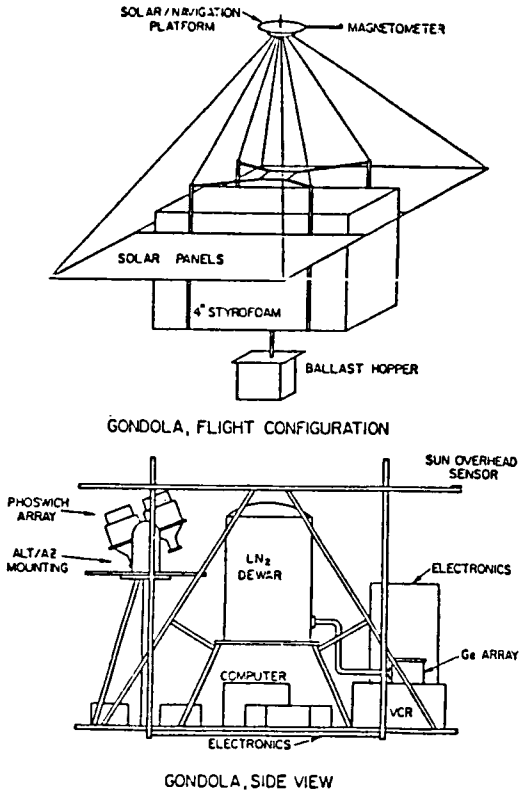

Figure 1. Schematic and perspective view of payload.

a 160 liter liquid nitrogen dewar is mounted in the center of the gondola where the nitrogen usage has no effect on the overall balance. The computer, the various instrument support modules, and the batteries are mounted on the floor of the inner frame. Two water-ballasted panels on the long sides of the inner frame provide heat sinking for the heat dissipating units such as the servo amplifiers and the various transmitters used on the gondola. The primary purpose of the water ballast is to maintain an acceptable minimum nighttime temperature for the electronics. During the day, excess solar panel power is used to reheat the water if necessary.

3.1. Ballast System

To maintain altitude for the flight, and to insure against extremely cold thunderstorm cloud conditions, the 2100 lb gondola with parachute was accompanied by an additional 900 lbs of ballast at launch. The ballast hopper is suspended below the gondola from the outer frame. An automated ballast release system, controlled by altitude sensing equipment, was provided by the National Scientific Balloon Facility (NSBF).

3.2. Power System

The power system consists of approximately 167 sq. ft. of solar panels, a battery charge regulator, a 28-volt stack and a 12-volt stack of lead-acid gel batteries (see Figure 2). The solar panel area consists of two fixed 4 ft. by 5 ft. panels and two retractable 5-1/3 ft. by 12 ft. panels. The retractable panels are hinged upwards during launch and lowered with a winch and cable system by radio command immediately after launch. The solar cells are wired as 7 strings of 37.5 volts and 7 strings of 15 volts with each string supplying 2 amperes of current at full sunlight. The charge regulator operates by disconnecting successive solar cell strings as the batteries reach full charge in order to avoid overcharging and damaging the batteries. The excess power is used for heating thermal ballast. The batteries consist of two strings each of 33 amp-hr cells in parallel. The 28-volt stack is used for all experiment and servo power while the 12-volt stack is used by the NSBF support systems such as the GOES and ARGOS transmitters and the altitude control system. The experiment and servo systems consume approximately 90 watts continuously.

3.3. Pointing, Navigation, and Tracking System

To conserve power, only those detectors that are highly directional are actively pointed. The rest of the gondola rotates with the balloon. For direction reference, a small platform equipped with several optical sensors and magnetometers is mounted above the gondola (see Figure 2). A servo system rotates the platform to track the sun in azimuth for solar elevation angles of 0 to 82°. An optical sensor with a 16° opening angle is mounted on top of the gondola pointed vertically upward. This sensor signals the platform control when the sun is within 8° of overhead. At such elevation angles the azimuth sensor is unreliable and therefore magnetic pointing is preferred. For sun angles higher than 82° or at night, the platform is rotated to point to magnetic north. The azimuth angle of the platform relative to the gondola is read out with a shaft encoder and a potentiometer. An elevation sensor is mounted on the shaft of a gearmotor which in turn is mounted on the platform. A servo system enables the sensor to track the sun in elevation and a potentiometer reads out the elevation shaft angle. When the sun is higher then 82° the elevation servo points straight up and at night the servo points to the horizon.

An additional sensor with a larger opening angle and a high precision clock are utilized by the navigation software in the computer to determine the latitude and longitude of the gondola. The precise time of sunrise and sunset in the field of view of this sensor are used as follows: when corrected for velocity, the average of the two times (i.e., local noon) determines longitude while the total time in the field of view determines latitude.

Additional navigation data for use on the ground are provided by the ARGOS system. A low power transmitter, supplied by NSBF, periodically transmits a burst of data containing altitude and housekeeping data. A passing satellite determines position by Doppler shift of the carrier signal. This information is downloaded to tracking stations and sent to NSBF via telex.

The readouts from the platform and navigation sensors are routed to the control computer and to the collimator control. The computer estimates the balloon location

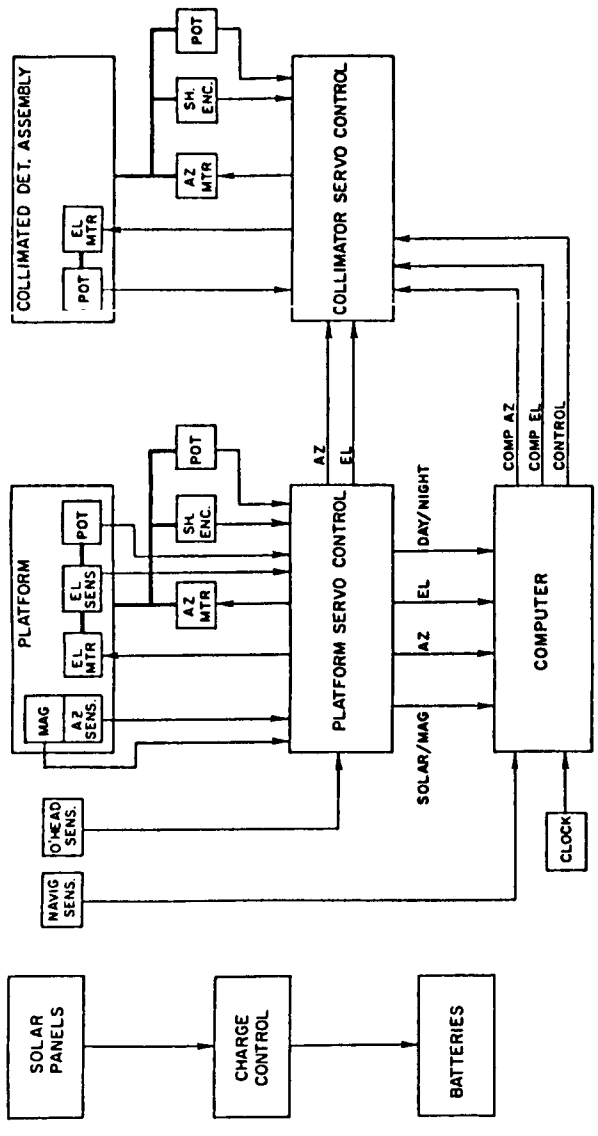

Figure 2. Block diagram of balloon systems.

GONDOLA POWER AND POINTING SYSTEM

and corrects for deviations of the earth's magnetic field in computing pointing directions for the non-solar targets. An alt-azimuth mount inside the gondola carries the collimated detector assemblies and orients them relative to the platform according to a viewing program in the control computer. During times when the program does not require offset pointing, i.e., when observing the sun, the elevation and azimuth servos drive the collimator axes such that their shaft readouts agree with those from the platform. At times when offset pointing is required, the computer calculates collimator shaft angle values from ephemeris data and platform shaft angles; a control line from the computer causes the collimator servos to switch from platform inputs to computer inputs.

4. DATA SYSTEM

The data system is designed to work independently for long periods (20 days or more), during which time its tasks include: collecting data from the detectors, compressing it for storage and transmitting it to geosynchronous spacecraft or to the ground. In addition, the data system also generates pointing information for the phoswich collimator using navigation information obtained from a solar eclipser; monitors detector rates to generate burst triggers, which are used to control the data collection modes; monitors the various housekeeping data and auxiliary detectors, and adds data from these sources to the various telemetry streams. Figure 3 shows a block diagram of the data system.

The input rate from the detectors is highly variable, from tens to tens of thousands of events per second. Events consist of 10-12 bits of pulse height and pulse shape information. The data system must record each event together with detector identification information. In addition, time-tags must be appended to the data every few events. Other input information that must be recorded periodically include various rates, and housekeeping information, such as temperatures and pointing directions. The expected total data volume consists mainly of the background rate (tens of events per second), integrated over the duration of the flight. Depending on the length of the flight, the expected data volume is in the hundreds of megabytes.

4.1. Central Processor

Due to the long duration of the flight, the data system has a limited power budget (about 10 watts), which includes a large memory array and a tape recorder. This requires the use of low power devices and power switching when possible. The data system is maintained at near room temperature, but must operate at high altitude (except the tape recorder, which is in a pressure vessel).

The wide variety of complex tasks required by the data system immediately suggests the use of an on-board microprocessor. The size of the event words (16 bit), the requirement for a large memory addressing space, and a fairly heavy processing load all indicate the use of one of the newer 16 bit microprocessors. Power considerations dictate a CMOS design. Together these requirements narrow the field down considerably. For budgetary reasons, the use of an existing commercial single board computer is desirable. For these reasons, the data system is based on a multibus configuration, with an 86C/05 single board computer as the control unit. The 86C/05 contains a Harris 80C86 CMOS microprocessor, together with CMOS bus control circuits, memory, interrupt con-

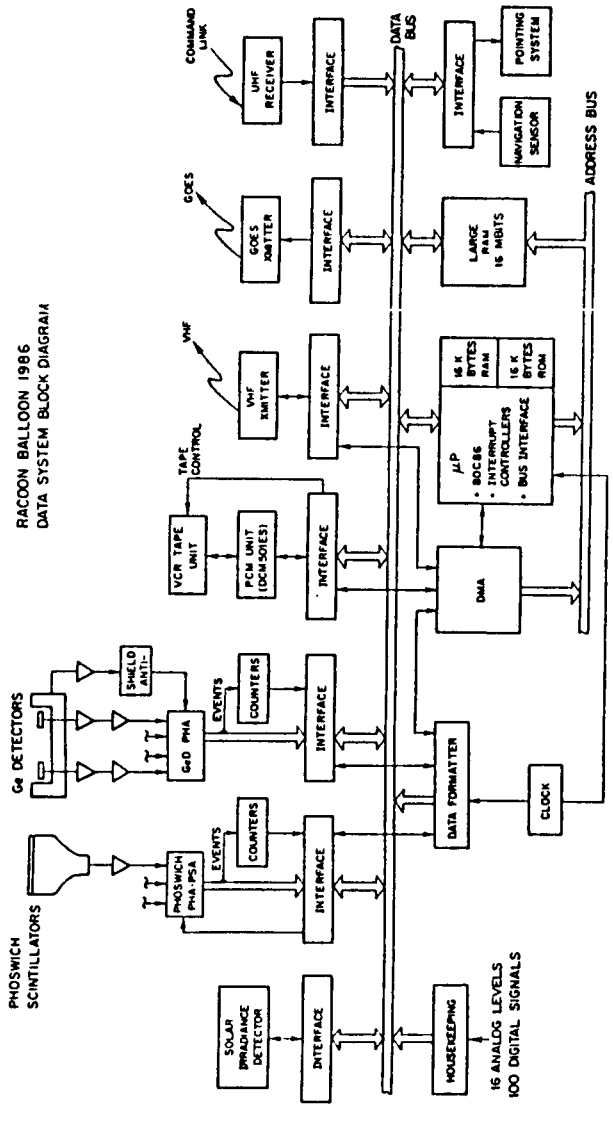

Figure 3. Block diagram of data system.

troller, etc. The rest of the data system is fabricated on wirewrap multibus cards, which are connected together and to the CPU bus via a modified multibus back-plane.

4.2. Data Collection

The large range of event rates, together with the need to compress the data, suggest the use of asynchronous data collection. Each event includes a detector identifier so that data from the various detectors can be mixed freely. A fixed number of events are packaged together into a fixed format, with time tags added every 14 events, and various rates and housekeeping information also included. This scheme has the advantage that during high event rates, high time resolution is available without wasting data space during low event rates. Because of the relatively high maximum event rate, the events are formatted and put into memory with little CPU intervention, by means of Direct Memory Access (DMA).

4.3. Data Storage

A high density tape recorder is required to store the large volume of data generated. A commercial portable VCR unit is used together with a PCM board removed from an audio digitizer (Sony PCM 501ES). This scheme is similar to that described by Althouse and Cook (1985), and provides gigabytes of storage. The data are collected into a large Random Access Memory (RAM) and are written off to tape when a certain data volume has been collected. The selection of the size of the large RAM is constrained by a number of parameters. Power considerations require that the tape be turned on fairly infrequently. The tape unit is unformatted, so data must be written in fixed-size blocks, with large gaps for starting and stopping the tape. In order for these gaps not to dominate the tape usage, the block size should be larger than the gap. Also, the RAM is sized so that, if a burst occurs while the tape power is off, it is unlikely that the RAM will overflow before the tape can be re-started. In addition, the RAM is used to store a limited volume of bursts for transmission to GOES/METEOSAT. Together these requirements give a RAM size of 2 megabytes or more. This large RAM was implemented using commercially available memory modules (IBM PC expansion modules) containing many 64 kilobit dynamic RAMs for a total capacity of 2 megabytes. The capacity can easily be expanded to 8 megabytes by replacing the RAMs with 256 kilobit chips.

4.4. Data Transmission

For most of the duration of the flight, the balloon is out of range of the ground VHF/UHF receiving station for high-rate data. The only real-time data link is via the GOES satellites, with about 60 bits-per-second (bps) telemetry capability. The satellite telemetry link is used to obtain limited real-time data and event data. The bulk of the data must be stored on-board for down-link when the balloon comes back into line-of-sight communications. Thus the data system must interface to and generate data for both the GOES transmitter and a VHF/UHF high bit rate transmitter. The VHF/UHF transmitter will be run in two modes: 256,000 bps rate for dumping data to the ground station at the end of the flight, and 8000 bps rate for monitoring the data in real-time at the beginning of the flight, before the balloon goes out of range.

The data system has interfaces to both the GOES transmitter and a VHF/UHF

transmitter. The VHF/UHF transmitter runs at a fairly high rate, and so DMA is used to avoid over-burdening the CPU. The data are stored in memory and tape by the data collection system in a format suitable for transmission (including sync words, frame counter, etc.) so that the data may be sent directly without modification. The GOES data are formatted by the CPU since it has such a low bit rate.

5. FLIGHT PERFORMANCE

The payload was launched at ~2100 UT February 9, 1987, from Alice Springs, Australia. Due to a malfunction of the ballast control system all 900 lbs of ballast were dropped at launch. The balloon thus flew as an unballasted RACOON for the entire flight. With the loss of ballast the ascent was extremely rapid (~1500 ft./min), and the balloon reached a float altitude of ~132,000 ft.—i.e., ~2000 ft. higher than normal. Some of the helium was vented, and perhaps some leaks developed from the stress of the rapid ascent.

Figure 4 shows the balloon altitude versus time. The daytime float altitude generally decreased throughout the flight. Preliminary analysis indicates that helium was lost at a rate of ~1-2% per day, possibly from a small leak. The gas temperature, and therefore the float altitude, are determined primarily by the radiation the balloon receives from the sun and the earth. Cold storm clouds below the balloon are responsible for the sharp drops in altitude superimposed on the general long-term decrease. Ballast drops totaling ~10-15% (600-900 lbs) of the total balloon plus payload weight would have kept the daytime balloon float altitude near 130,000 ft. for the entire 12 days.

The trajectory of the balloon is shown in Figure 5. The balloon started westward at an average rate of ~30° longitude per day (~130 km/hour), but slowed down as the balloon altitude decreased. The payload was commanded to cut down over Brazil after 12 days, and was recovered with relatively minor damage.

All the detectors, the experiment data system, and electronics appeared to have functioned perfectly. The data transmission to the GOES spacecraft appears to have been intermittent. Only ~10% of those data have been recovered. All of the data, however, were stored in the on-board VCR tape. Analysis of those data is underway. Figure 6 shows a preliminary 30-minute raw counts spectrum from a single germanium detector. Prominent background line features can be seen at 511, 198, and 140 keV. The sun is in the detector field of view at this time.

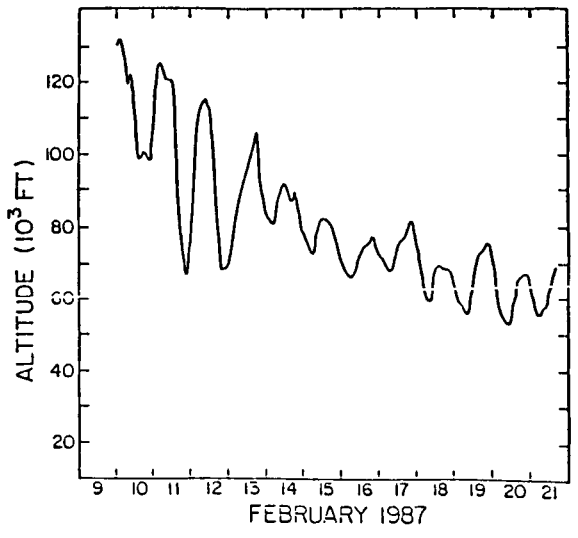

Figure 4. Balloon altitude versus time obtained via GOES and ARGOS data transmissions (courtesy NSBF).

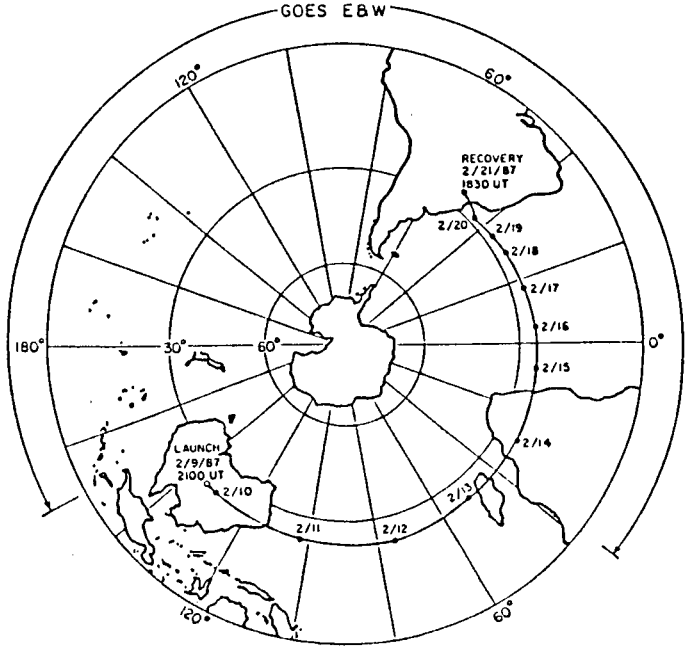

Figure 5. Trajectory of balloon flight from ARGOS tracking data (courtesy NSBF).

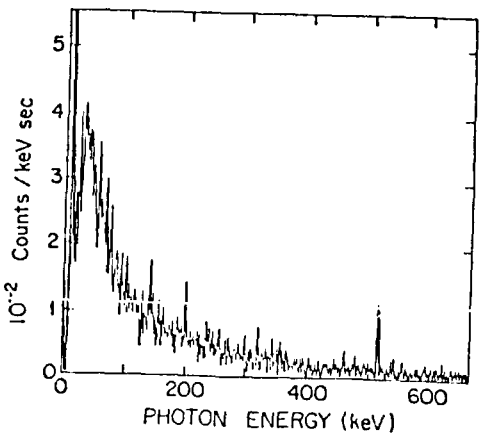

Figure 6. Sample count rate spectrum from a single germanium detector during 30 minutes observation of the quiet sun.

ACKNOWLEDGMENTS

NSBF personnel provided the launch and recovery of the payload and supplied the GOES and ARGOS transmitters and ballast system. D. Peacock at NSF and G. Frye and his group at Case Western Reserve provided much needed advice and support. This research was supported in part by NSF grant ATM-8402231 and NASA grant NAGW-516.

REFERENCES

Althouse, W. E. and Cook, W. R: 1985, in F. C. Jones *et al.* (eds.), *19th Internat'l. Cosmic Ray Conf. Papers, NASA Conf. Publ.* **2376**, Vol. 3, p. 395, NASA, Washington, D.C.

Cotin, F., deJager, C., Henoux, J.-C., Heise, J., Hilhorst, M., Hurley, K., Niel, M., Paschmann, G., Sommer, M., Van Rooijen, J., and Vedrenne, G.: 1983, *ESA* SP-**1050**, 211.

Koga, R., Frye, G. M., Jr., Owen, A., Denehy, B. V., Mace, D., and Thomas, J.: 1985, in F. C. Jones *et al.* (eds.), *19th Internat'l. Cosmic Ray Conf. Papers, NASA Conf. Publ.* **2376**, Vol. 4, p. 142, NASA, Washington, D.C.

Lally, V.: 1982, *Proc. XXIV COSPAR Conf.*, Ottawa, I, p. 1.4.

Lin, R. P., Schwartz, R. A., Pelling, R. M., and Hurley, K. C.: 1981, *Astrophys. J.* **251**, L109.

Matteson, J. L., Nolan, P. L., Pacieses, W. S., and Pelling, R. M.: 1977, *Space Sci. Instr.* **3**, 391.

Appendix C
Previous LDBF Flight Systems

Here, we describe two flight systems already developed and flown by our investigator team which form a strong technical basis for the support systems needed to attain our Max '91 objectives.

The LDBF '87 Gondola

This payload, described in detail by *Lin et al.*, "A long duration balloon payload for hard X-ray and gamma-ray observations of the Sun" (appended), was developed explicitly for the study of transient solar phenomena. The successful flight of this system demonstrated the feasibility of the technical approaches used in its design and indicated the promise for long duration balloon flights as a solar observation technique.

The LDBF '88 Gondola

The occurrence of supernova 1987a in February 1987 (SN 1987a) presented a unique opportunity to study explosive nucleosynthesis as well as the dynamics of the supernova process. However, the transient nature of the event demanded that observations be conducted as soon as possible with special emphasis on observing the evolution of the γ-ray flux during the first one to two years. On this basis it was decided to assemble a long duration payload which would provide observations using existing instruments. The system would include the phoswich scintillator array from the previous LDBF payload and a shielded germanium detector system currently under preparation for a test balloon flight. These instruments would be interfaced to the existing LDBF system. New mechanical subsystems would be developed to support the existing detector and the existing LDBF computer and software would be adapted to control the new gondola. As originally conceived very little new development would be necessary. This was fortuitous, since the entire payload would have to be fabricated, tested and shipped to Australia within 7 months if the February 1988 launch window were to be met.

Gondola Description

The LDBF88 gondola was designed to meet the unique requirements imposed by the SN 1987a opportunity, the detector systems to be used in the observations, and the long duration balloon flight operation.

Detector platform. The fundamental mechanical requirement of the LDBF88 gondola was to provide co-aligned pointing for the tandem detector components while supporting an unusually large ballast load, as well as solar panels and an independently orientable communications dish. This was accomplished by mounting the two detector systems on a detector platform which was movable in azimuth around a central load-bearing column. The detector platform also provided an elevation gimbal to give the needed 2-axis orientation freedom. The detector platform also carried a reserve LN_2 dewar for replenishment of the small germanium detector coolant supply. All electronics systems were carried on an electronics platform, fixed to the central column below the detector platform. This layout is shown schematically in Figure F1 and illustrated in a model of the internal gondola assembly shown in Figure F2.

Thermal control. For thermal control, the entire internal assembly was contained within an insulating chamber fabricated in the approximate shape of a cube, ~2 m on a side. This primary thermal control system is designed to use the ambient electronics dissipation to maintain an environment between 0 and 30°C through balloon night and day operation. Additional "secondary" thermal control is provided to the phoswich scintillation array by thermally isolating it from the internal gondola assembly and enclosing it in its own insulation chamber. Thermostatically controlled heaters are then provided within the phoswich chamber to maintain its temperature within 20 to 30°C.

Aspect platform. As noted above, the detector platform is driven in azimuth against the electronics platform. To provide aspect reference a third platform is provided above the detector

ORIGINAL PAGE IS
OF POOR QUALITY

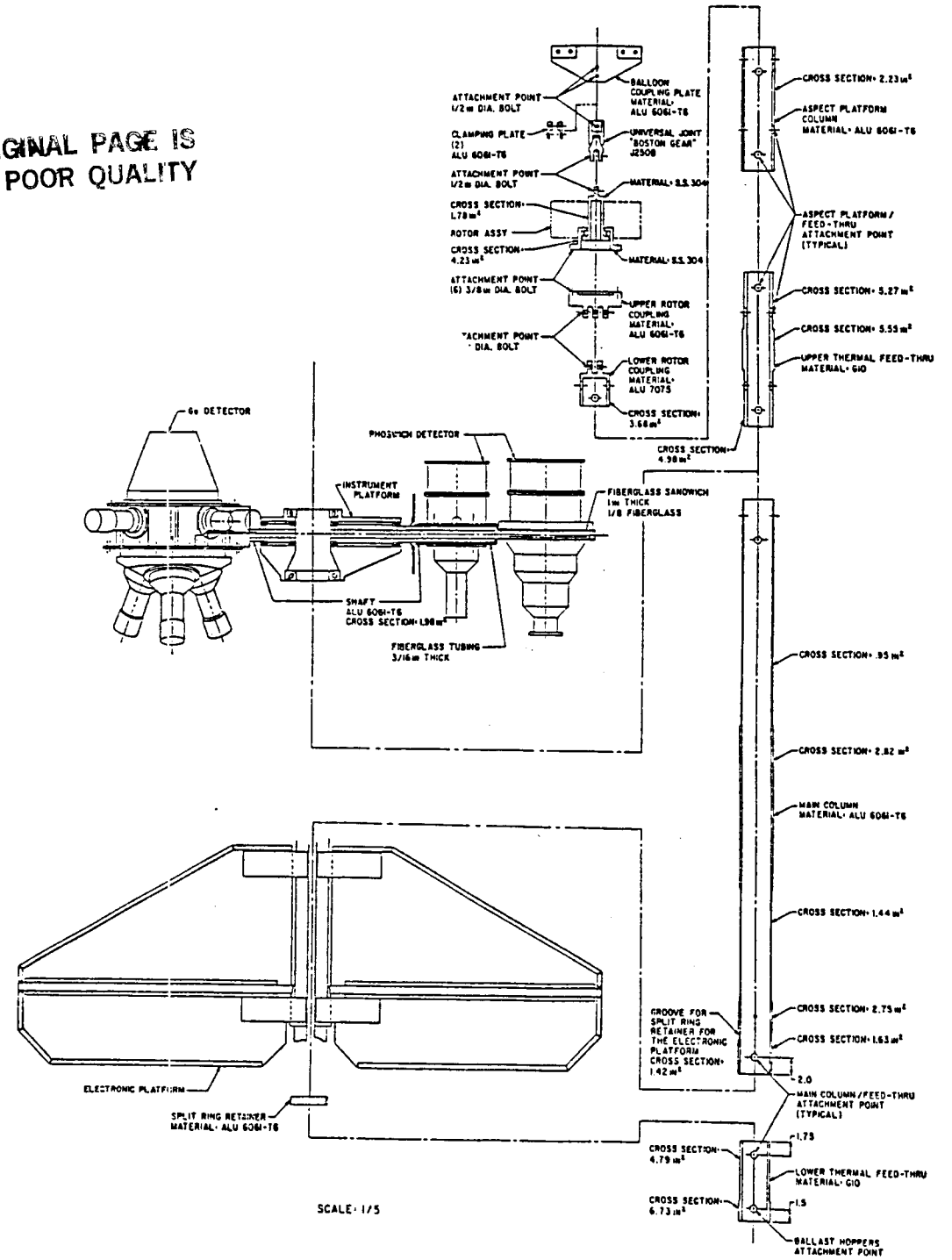

Figure F1. Load path schematic. This drawing indicates the relationship of the principle mass elements in the LDBF88 flight system. The in-line central structure was a particularly efficient design for carrying the ballast hopper (up to 1500 lbs.) and providing a compact gimbal for the tandem detector array.

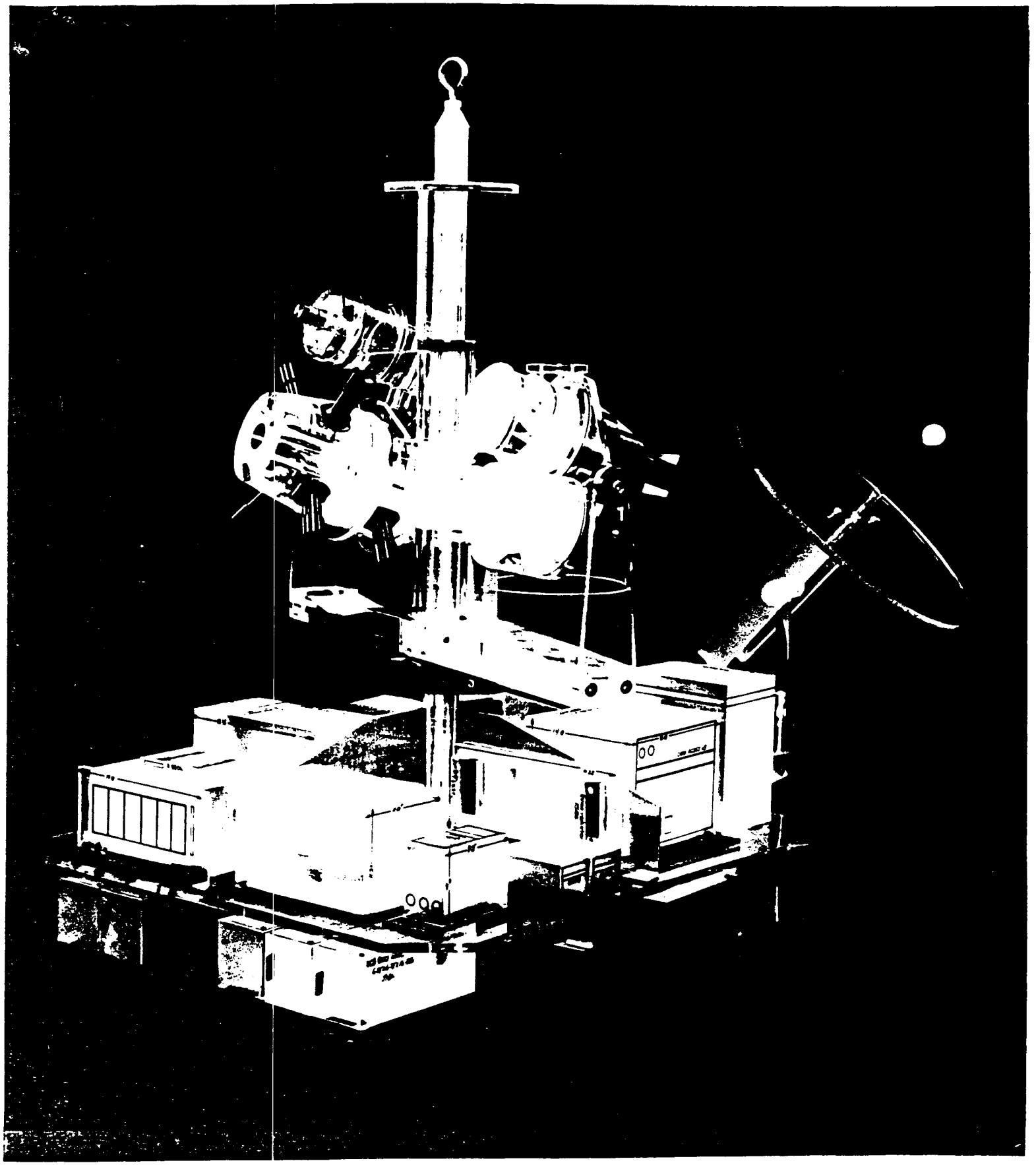

Figure F2. A model of the LDBF88 internal gondola. This illustrates the relationship of the detector gimbal to the electronics and aspect platforms. The mounting of the INMARSAT 1-m dish is also indicated. This assembly (excluding the antenna and aspect platform is carried within a thermal control enclosure).

assembly to mount a solar tracking sensor and magnetometer assembly. This "aspect platform" co-rotates with the detector platform with its sensor outputs in a closed loop with the azimuth drive motor. Thus, the azimuth servo is configured to either maintain the solar tracker on the sun azimuth position, or alternatively, maintain the reference magnetometer at null. Finally, the aspect platform may, under control of the central processor, be moved to an arbitrary offset position relative to the detector platform. This provides capability to orient the detector platform to any desired position relative to either the solar or magnetic reference. For elevation control, a second solar elevation tracker is mounted on the aspect platform. This device, similar in concept to the azimuth tracker, uses a simple shadow-vane/photodiode sensor arrangement to track the solar elevation angle. The detector elevation servo is then synchronized with the solar elevation sensor to follow the sun in elevation. Figure F3 shows the internal gondola undergoing angular alignment prior to enclosure in the thermal box.

External Gondola. Additional components, mounted in fixed relation to the electronics platform include the solar panels, the communications antenna, and the ballast hopper. These systems were carried by the internal gondola through thermally isolated mounts which penetrated the insulation cube. Figure F4 shows the complete gondola with the solar panels folded, suspended from the launch vehicle.

Weight Breakdown. A critical aspect of the LDBF88 system was the overall system weight. In addition to using a weight efficient configuration requiring a minimum of structure, key elements of the LDBF88 system were designed for minimum weight using novel materials and designs. The electronics platform was fabricated using aluminum honeycomb for high strength and rigidity. The primary thermal enclosure box was constructed from urethane foam (thermal conductivity ~1/2 of "conventional" styrofoam per unit weight). The enclosure was carried by the electronics platform through a foam core fiberglass superstructure which also carried the solar panels. The solar panels were constructed using ultra-thin wall tubing frames with fiberglass mesh for mounting of the solar cells. These structural elements proved to be remarkably durable, sustaining practically no damage through cutdown and impact of the gondola. Table F1 gives a breakdown of the LDBF88 subsystem weights as flown.

Table F1. LDBF88 Gondola Weight Breakdown

Detectors and LN supply:	454.5 lbs.
Structural components:	199.0
Thermal control components:	195.0
Electronics:	278.0
Batteries:	290.0
Misc. mechanical:	105.5
Solar panels:	105
NSBF mechanical:	462.5*
NSBF electronics:	62
Total flight system:	2150 lbs. (w/o ballast)

* Including 191 lbs. for extra heavy duty parachute and rigging

The overall electrical design of the LDBF88 gondola was largely derived from the original LDBF system described in detail by *Lin et al.* (1987). That system utilized a single board computer organized around a Harris 80C86 microprocessor. For brevity we will not repeat the description of that system, but only describe the significant modifications which were incorporated into the LDBF88 system.

INMARSAT. In order to provide real time bi-directional contact a one-meter antenna which operates via the INMARSAT shipboard communications system was incorporated into the flight system. This unit, procured from a commercial vendor and adapted to operate in a balloon environment, would essentially provide a telephone link to the gondola processor with simple modem interface operated at 1200 baud. Other modifications to the gondola processor system, described below, were required to support the system.

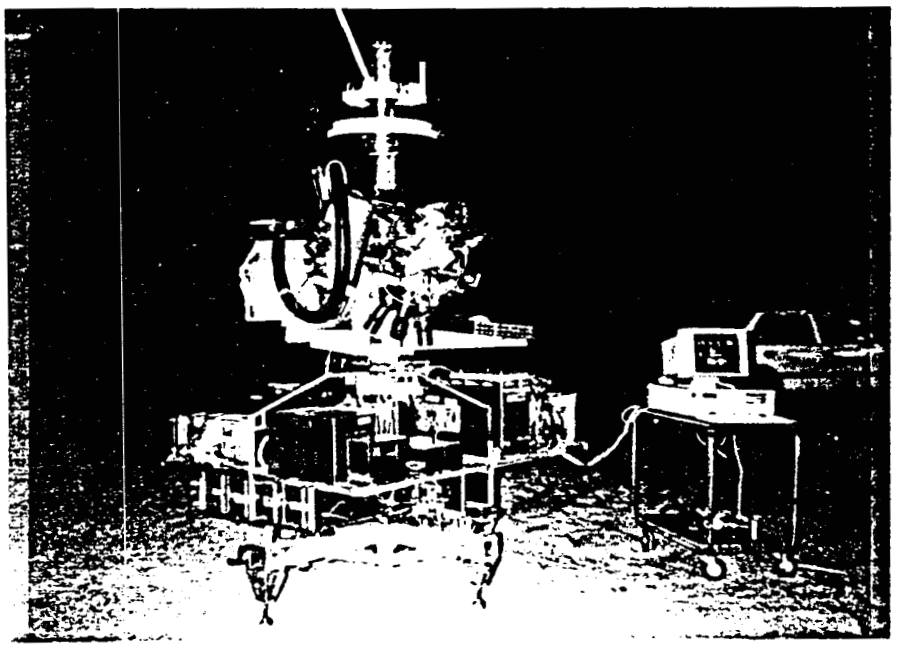

Figure F3. Internal gondola alignment operation. The internal gondola is shown here during alignmnent of the aspect platform relative to the detector platform. Both solar and magnetic references are calibrated to permit day and night operation.

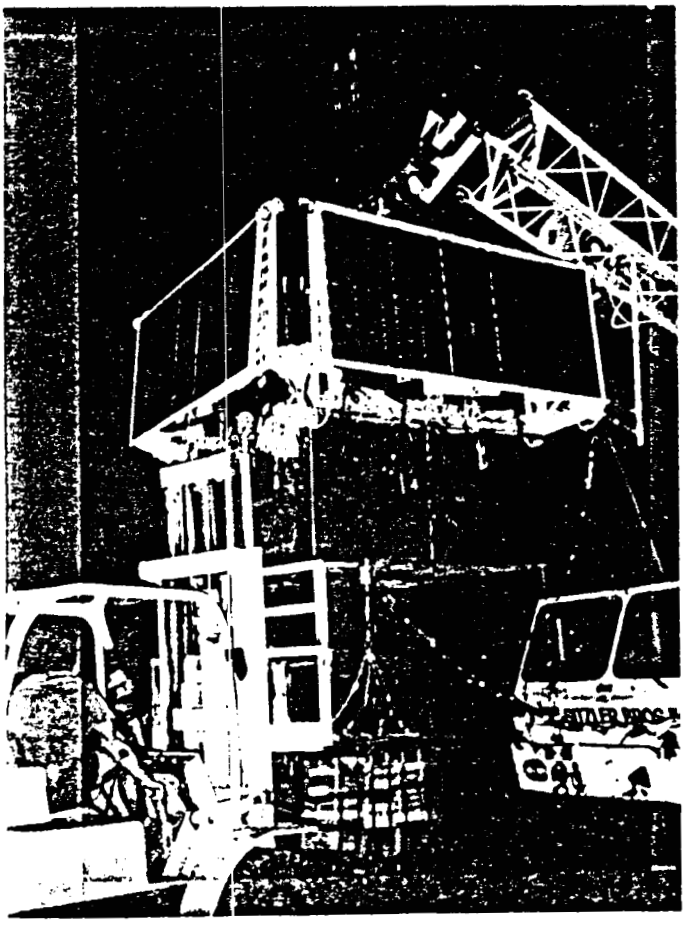

Figure F4. Flight system on launch vehicle. The complete gondola including thermal enclosure, solar panels (folded), and ballast hopper is shown being prepared for a February 1988 launch. Preparation of the INMARSAT antenna was not completed in time for the unit to be included in the payload for this flight.

Transit/Omega. This system, supplied; by NSBF, is a hybrid of two complementary navigation systems, designed to provide essentially constant Omega positional information with periodic initialization updates via the Transit satellite system. Geographic position data generated by the system were read directly into the gondola processor to assist in celestial navigation computations. Since the Transit/Omega system was considered to be developmental, back-up navigation data would be provided via the solar transit detection system carried over from the original LDBF gondola. The on-board computer would be instructed via ground command (either link-of-sight or INMARSAT) as to which navigation system should be referenced by the celestial navigation program.

On-board Computer. The 86C86 single board computer was modified by doubling the available RAM to 4.0 Mbytes. This enhancement was required to support additional data management tasks introduced by the use of the INMARSAT system. Accordingly, there were substantial modifications required to the flight software package to generate the INMARSAT data base, format it for output, and perform the required antenna control functions for establishing ground contact and interacting with the ground computer.

Other modifications incorporated in the flight system included: a) increasing the solar panel area to provide 1325 watts available power for 24-hr. operation of the system; 2) a three-stage ballast control system, provided by NSBF; and 3) a nitrogen replenishment system for periodic refill of the germanium dewar.

Appendix D

Long Duration Balloon Flights (LDBFs)

HIREGS is designed to use the standard 28.4 million cu. ft., 3000 lb. nominal (3700 lb. maximum) payload capability balloon which has been used for long duration balloon flights (LDBF) in the past two years. Four mid-latitude flights have been completed successfully with this balloon, two each in early 1987 and early 1988. All the flights were launched from Alice Springs, Australia, and proceeded westward to South America, where the payloads were recovered. Flight durations ranged from 6 to 12 days, with the longer flights due to lower float altitudes.

Our group designed and fabricated the scientific payloads for two of the flights, one in each year. In 1987 we flew hard X-ray and low energy gamma-ray instrumentation for solar observations (see *Lin et al.*, 1987). An auto-ballast system malfunction dumped all the ballast at launch, so the balloon flew as an unballasted RACOON (RAdiation COntrolled balloON), i.e., the balloon rose in the daytime and sank at night. The daytime float altitudes monotonically decreased, due to loss of lift with time. Calculations based on standard atmospheric models indicate that ~2.5–3% lift was lost each day-night cycle. For a 7-day flight (six nights) this implies that 15–18% of total (payload plus balloon) weight is required in ballast (1050–1300 lbs.) to maintain the initial daytime float altitude of ~126–130K ft. through the flight. If an additional ~200 lbs. ballast is carried for emergencies this leaves ~2200–2450 lbs. for payload, sufficient for an instrument such as HIREGS. Longer flights, perhaps around the world, are possible but the latter part of the flight would be as an unballasted RACOON with decreasing float altitudes. This may be an acceptable method for extending solar gamma-ray observation time by ~3 days since the gamma-rays will penetrate to ~10^5 ft. altitude.

Antarctic Flights

An attractive alternative is provided by flights in Antarctica during its summer. A 11.6 million cu. ft. balloon with a ~2390 lb. payload was successfully launched in January (1988) from near McMurdo (78° latitude) (*Rester et al.*, 1988). After 65 hours the payload was cut down because of a power supply failure. The balloon drifted westward approximately along the 78° latitude line and came down near Vostok, about 80° west of McMurdo. Based on the information from this flight, the primary advantages of Antarctic flights are:

1. 24 hour/day solar observations;
2. *Much* longer flights are possible. Lift loss of less than 0.5%/day was observed in this flight. Thus 15% of total payload weight in ballast would last 30 days, compared to 7 days at mid-latitudes.
3. No problems with crossing international boundaries;
4. Essentially no risk of accidental landing in a heavily populated area, or in an ocean.

Since the Sun would always be relatively low in the sky the photon transmission through the atmosphere would be lower than at mid-latitudes, but by only ~10–25% (averaged over 12 hours mid-latitude, and 24 hours for Antarctica) at gamma-ray line energies (see Figure D1). Leakage background would increase because of the lower geomagnetic cutoff in Antarctica. Data from the January 1988 flight, however, indicate that with good shielding the background increase is not a major problem (see *Rester et al.*, 1988).

Long Antarctic flights thus appear to be ideal for catching the large flares which have strong gamma-ray line emission. Such large flares would also provide the count rate statistics needed for detailed hard X-ray images at high time resolution and for physically meaningful polarization measurements, observations which might be made by other Max '91 balloon instruments. Also, Antarctic flights are advantageous for possible Max '91 optical as well as hard X-ray fine imaging, in that the Sun can always be observed without looking through the balloon.

In the January 1988 Antarctic flight the payload was recovered by a ski-equipped airplane. Recovery may not be feasible over some parts of Antarctica. On the other hand, $\gtrsim$75% of mid-latitude flights are over oceans where recovery would not be possible either.

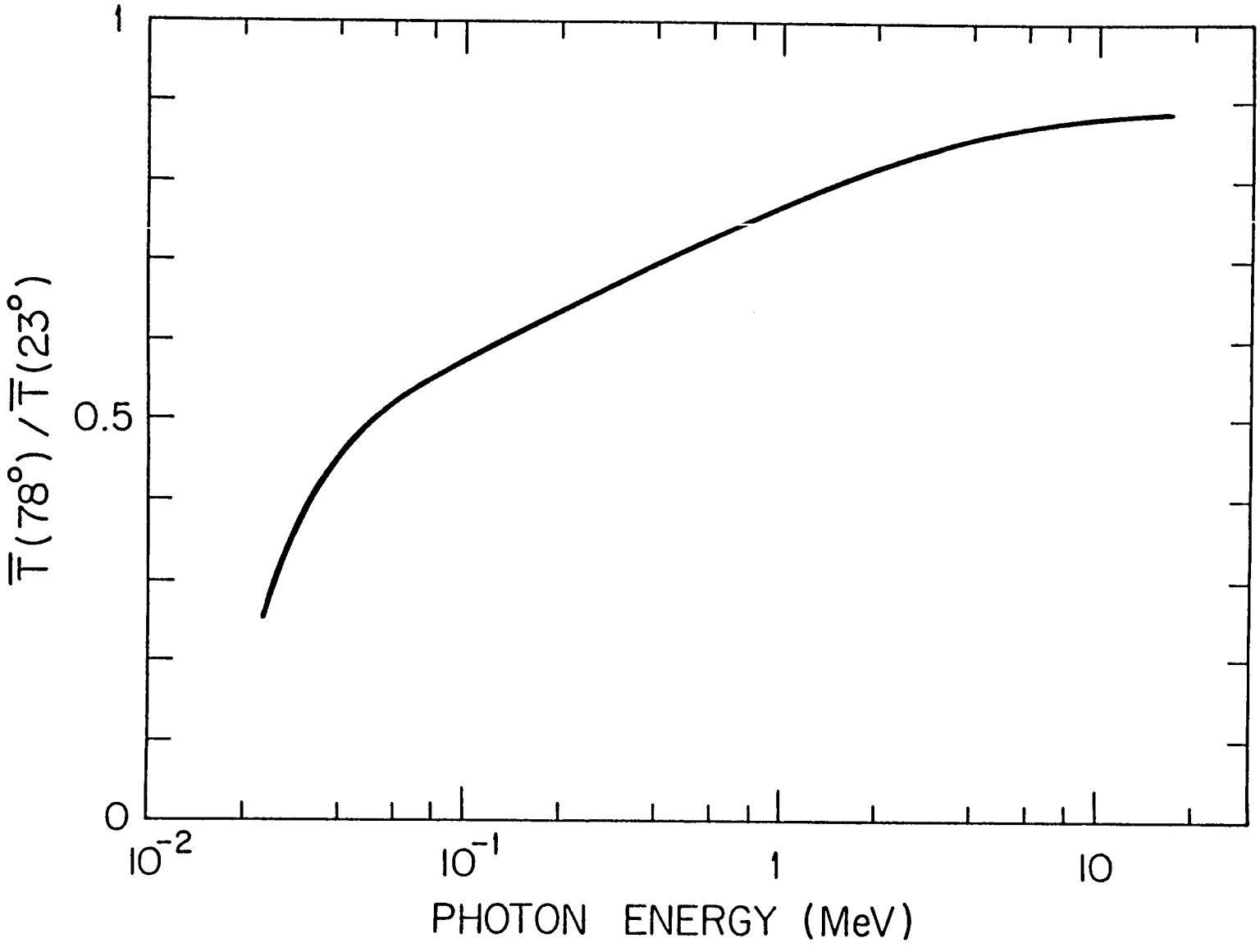

Figure D1. The ratio of atmospheric transmission at Antarctica (McMurdo, 78° latitude) to that at mid-latitudes (23° latitude) for solar observations during summertime, averaged over the day (12 hours mid-latitude, 24 hours Antarctica).

With the wind at float altitudes flowing typically along latitude lines, an intriguing possibility is to launch balloons from the South Pole. The balloons should then stay near the South Pole and a single ground station could provide continuous line-of-sight telemetry. At present, however, only small $1\text{–}2\times10^5$ cu. ft. balloons have been hand launched from South Pole. Equipment and techniques would need to be developed for launch of large balloons and heavy payloads. Our group at UCB is planning South Pole launches of ~300 lb. payloads with $\sim3\times10^6$ cu. ft. balloons in December 1989/January 1990.

Northern Hemisphere Flights

Southern hemisphere LDBFs are only possible in the December-February summer season. Northern hemisphere LDBFs offer the possibility of coverage in the June-August northern summertime. This is particularly attractive since most of the ground-based solar observatories are located in the northern hemisphere, and they are able to obtain the most extensive solar coverage in summertime.

LDBFs have been made from Sicily to the U.S. in the past. The prevailing winds, however, will bring the balloon over the heavily populated eastern seaboard of the U.S. An alternative would be to launch from the west coast of the U.S. and recover the payload in China. The Chinese have had extensive experience in scientific ballooning and are presently involved in a cooperative program with Japan, where balloons are launched from Japan and the payload recovered in China. They are eager to collaborate in U.S.-China LDBFs as well. Such LDBFs could provide flight times comparable to Australia-Brazil. Mid-latitude northern hemisphere LDBF possibilities definitely need to be explored for Max '91.